Supplementary information

Optical control of neuronal firing via photoinduced electron transfer in donor-acceptor conjugates

Yuta Takano,[1] Tomohiro Numata,[2,3] Kazuto Fujishima,[1] Kazuaki Miyake,[4] Kazuya Nakao,[4] Wesley David Grove,[1] Ryuji Inoue,[2] Mineko Kengaku,[1*] Shigeyoshi Sakaki,[5] Yasuo Mori,[3*] Tatsuya Murakami,[1] Hiroshi Imahori[1,4]*

[1]Institute for Integrated Cell-Material Sciences (WPI-iCeMS), Kyoto University, Sakyo-ku, Kyoto 606-8501, Japan.

[2]Department of Physiology, Graduate School of Medical Sciences, Fukuoka University, Nanakuma 7-45-1, Johnan-ku, Fukuoka 814-0180, Japan.

[3]Department of Synthetic Chemistry and Biological Chemistry, Graduate School of Engineering, Kyoto University, Nishikyo-ku, Kyoto 615-8510, Japan.

[4]Department of Molecular Engineering, Graduate School of Engineering, Kyoto University, Nishikyo-ku, Kyoto 615-8510, Japan.

[5]Fukui Institute for Fundamental Chemistry, Kyoto University, Sakyo-ku, Kyoto 606-8103, Japan.

*Correspondence to: imahori@scl.kyoto-u.ac.jp (H. I.); kengaku@icems.kyoto-u.ac.jp (M. K.); mori@sbchem.kyoto-u.ac.jp (Y. M.)

Materials and methods

Materials:

C_{60} (99.98%) was obtained from MTR Ltd. and compound **7** was purchased from Tokyo Chemical Industry Co., LTD. and used as-received. All other solvents and chemicals were of reagent-grade quality, purchased commercially, and used without further purification unless otherwise noted. Thin layer chromatography (TLC) and column chromatography were performed with Silica gel 60 F254 (Merck) and SiliaFlash F60 (230 – 400 mesh; SiliCycle Inc.), respectively. Dulbecco's phosphate buffered saline (PBS) and Hank's Balanced Salt Solution (HBSS) were obtained from Thermo Fisher Scientific Inc. (MA, USA). Cell culture dishes and glass bottom dishes were purchased from Corning Inc. (MA, USA).

General procedures:

^{1}H NMR spectra were measured by a JEOL JNM-EX400 NMR spectrometer or a Bruker AVANCE 500 spectrometer, where TMS was used as an internal reference (δ = 0.00 ppm). Matrix-assisted laser desorption/ionization (MALDI) time-of-flight mass spectra were obtained using a SHIMADZU Biotech AXIMA-CFR with 1,8-dihydroxy-9(10H)-anthracenone (dithranol) as a matrix for a negative mode and a positive mode, respectively. IR spectra were recorded on a JASCO FT/IR-470 Plus spectrometer. UV–vis–near infrared (NIR) spectra were measured with a Perkin-Elmer Lambda 900 spectrometer. Dynamic light scattering (DLS) analyses were conducted with NIKKISO Nanotrac UPA-UT151. The data were averaged from three independent experiments. Steady-state fluorescence spectra were obtained by a HORIBA SPEX Fluoromax-3 spectrofluorometer or a HORIBA Jobin Yvon FluoroMax-4 spectrofluorometer. Statistical analysis was performed using Igor Pro v6.3 using a *one-way ANOVA* with a *Dunnett's* post hoc test for significance.

Synthesis:

Compounds **4**,[1] **5**,[2] **12**,[1] **14**,[1] **15**,[3] **16**,[4] **19**,[5] **20**[6] and **23**[1] were synthesized according to the literatures and were characterized with the spectral data therein.

Compound **13H$_2$**.[1]

A solution of C_{60} (14.4 mg, 20.0 μmol), **12** (12.4 mg, 8.48 μmol), and *N*-methylglycine (4.74 mg, 53.2 μmol) in toluene (46.0 mL) was refluxed under argon atmosphere in the dark for 15 h. The reaction mixture was allowed to cool to room temperature and then evaporated to dryness at reduced pressure. Flash column chromatography on silica gel with toluene/AcOEt = 20/1 (v/v) as the eluent and reprecipitation from $CHCl_3$-methanol afforded **13H$_2$** as a purple solid (15.0 mg, 6.78 μmol, 80% yield). ^{1}H NMR (300 MHz, $CDCl_3$): δ 8.90 (d, J = 5 Hz, 2H), 8.89 (d, J = 5 Hz, 2H), 8.80 (d, J = 5 Hz, 2H), 8.77 (d, J = 5 Hz, 2H), 8.70 (br.s, 1H), 8.36 (d, J = 7 Hz, 2H), 8.30 (d, J = 7 Hz, 4H), 8.22 (d, J = 7 Hz, 2H), 8.05 (d, J = 7 Hz, 4H), 8.04 (br.s, 1H), 7.97 (d, J = 7 Hz, 2H), 7.81 (s, 2H), 7.75 (d, J = 8 Hz, 1H), 7.59 (s, 1H), 7.11 (d, J = 8 Hz, 1H), 7.00 (d, J = 8 Hz, 2H), 6.99 (d, J = 8 Hz, 2H), 4.82 (s, 2H), 4.61 (d, J = 5 Hz, 1H), 4.44 (s, 1H), 4.31 (s, 2H), 4.18 (t, J = 5 Hz, 2H), 4.09 (s, 1H), 4.08 (s, 5H), 3.94 (s, 1H), 3.46 (t, J = 7 Hz, 2H), 2.70 (s, 3H), 2.15 – 1.90 (m, 4H), 1.73 – 1.22 (m, 40H), -2.79 (brs, 2H); FTIR (neat): *v* 3313, 3095, 2960, 2904, 2865, 2783, 1682, 1592, 1519, 1421, 1247, 973, 799, 718 cm^{-1}; HR mass (MALDI-TOF) calcd. for

$C_{153}H_{96}BrFeN_7O_3$ ([*M*]$^+$): 2213.611, found: 2213.610 *m/z*.

Compound **13Zn**.[1]

$Zn(OAc)_2$•$2H_2O$ (18.4 mg, 8.40 μmol) was added to a solution of **13H$_2$** (9.30 mg, 4.20 μmol) in toluene (3.3 mL) and stirred at room temperature overnight. Then, the reaction mixture was filtered and the filtrate was concentrated under reduced pressure. Reprecipitation from $CHCl_3$-methanol gave **13Zn** as a purple solid (8.5 mg, 0.0037 mmol, 90%). ^{1}H NMR (400 MHz, $CDCl_3$/MeOD = 1/1 (v/v)): δ 8.92 (d, J = 5 Hz, 4H), 8.81 (d, J = 5 Hz, 2H), 8.77 (d, J = 5 Hz, 2H), 8.25–8.11 (m, 8H), 7.99 (d, J = 6 Hz, 2H), 7.96 (br.s, 1H), 7.75 (d, J = 9 Hz, 2H), 7.70 (s, 2H), 7.59 (d, J = 8 Hz, 1H), 7.55 (s, 1H), 7.05 (d, J = 8 Hz, 2H), 6.99 (d, J = 8 Hz, 2H), 4.94 (Fc, s, 2H), 4.65 (d, J = 8 Hz, 2H), 4.22 (Fc, s, 2H), 4.50 (s, 1H), 4.01 (Fc, s, 5H), 4.01 (d, J = 8 Hz, 2H), 4.00 (d, J = 8 Hz, 2H), 3.61 (t, J = 7 Hz, 2H), 3.40 (t, J = 7 Hz, 2H), 2.62 (s, 3H), 2.10–1.82 (m, 4H), 1.65–1.10 (m, 40H); FTIR (neat): *v* 3440, 3095, 2960, 2904, 2864, 2982, 1683, 1593, 1558, 1519, 1421, 1247, 999, 797, 717 cm^{-1}; HR mass (MALDI-TOF): m/z calcd. for $C_{153}H_{94}FeBrN_7O_3Zn$ ([*M*]$^+$): 2275.524, found 2275.529.

Compound **1**.[1]

A solution of 33 wt.% NMe_3 in ethanol (0.03 mL) was added to a solution of **13Zn** (6.80 mg, 3.00 μmol) in $CHCl_3$ (1.0 mL) under stirring at room temperature and the reaction mixture was kept stirring for 3 days. During the reaction, $CHCl_3$ (1mL) and the NMe_3 solution (0.03 mL) were added every 24 h. Then, the reaction mixture was concentrated under reduced pressure and cyclohexane was added to yield the precipitate. The solid residue was washed with cyclohexane, cyclohexane/CH_2Cl_2 = 1/1 (v/v), then H_2O, followed by drying under a vacuum. The product **1** was obtained as a purple solid (5.8 mg, 2.5 μmol, 83% yield). ^{1}H NMR (500 MHz, DMSO-d_6, 70ºC): δ 10.35 (N*H*CO, brs, 1H), 10.29 (N*H*CO, brs, 1H), 8.90–8.70 (m, 9H), 8.45–8.30 (m, 6H), 8.26–8.20 (m, 2H), 8.07 (brs, 3H) 8.04–7.97 (m, 3H), 7.84 (brs, 2H) 7.82–7.78 (m, 2H), 7.68–7.61 (m, 2H), 7.05–6.95 (m, 2H), 4.86 (Fc, brs, 2H), 4.72 (brs, 1H), 4.69 (brs, 1H), 4.36 (Fc, brs, 2H), 4.09 (brs, 7H), 3.91 (brs, 1H), 3.35–3.30 (OCH_2, m, 2H), 3.07 (N$^+$(CH_3)$_3$, s, 9H), 2.67 (NCH_3, m, 3H), 2.62 (OCH$_2$CH_2, m, 1H), 2.35 (OCH$_2$CH_2, m, 1H), 1.83–1.72 (CH_2, m, 4H), 1.55–1.38 (m, 40H); FTIR (neat): *v* 3440, 3095, 2950, 2904, 2867, 2783, 1654, 1592, 1558, 1519, 1419, 1246, 996, 796, 717 cm^{-1}; HR mass (MALDI-TOF) calcd. for $C_{156}H_{103}FeN_8O_3Zn$ ([*M*-Br]$^+$): 2255.679, found: 2255.679 *m/z*. Note that the chemical shifts in ^{1}H NMR spectrum are not consistent with those in our previous report.[1] Since the compound was found to be decomposed at 100˚C in DMSO, the NMR signals have been reassigned in this study.

Compound **17**.

A solution of **14** (275 mg, 0.296 mmol), thionyl chloride (5 mL), and pyridine (5 mL) in dry toluene (50 mL) was refluxed for 2 h under argon atmosphere. The excess reagent and solvents were removed under reduced pressure, and the residue was dissolved in a mixture of dry toluene (50 mL) and pyridine (1.0 mL). Then **15** (197 mg, 0.444 mmol) and **16** (120 mg, 0.444 mmol) in toluene (5 mL) were added to the reaction mixture. The solution was kept stirring for 17 h at room temperature under argon atmosphere.

TLC showed three products and the second band was separated by column chromatography on silica gel with $CHCl_3$/AcOEt = 150:1 to 2:1 (v/v) as the eluent. The second fraction was concentrated and dissolved in a mixture of $CHCl_3$ (10 mL), trifluoroacetic acid (4.3 mL), and 5% aqueous sulfuric acid (3.3 mL). After stirring for 7 h, the mixture was poured onto 80 mL of water and extracted with $CHCl_3$. The organic layer was washed with saturated $NaHCO_3$ aqueous solution, dried over anhydrous $MgSO_4$, evaporated, and reprecipitation from CH_2Cl_2-methanol afforded **17** as a purple solid (34.2 mg, 0.0266 mmol, 9% yield). m.p. > 300ºC. ^{1}H NMR (400 MHz, $CDCl_3$): δ 10.03 (s, 1H), 8.94 (d, J = 5 Hz, 4H), 8.82 (d, J = 5 Hz, 2H), 8.81 (d, J = 6 Hz, 2H), 8.40 (d, J = 8 Hz, 2H), 8.38 (br.s, 1H), 8.34 (d, J = 10 Hz, 2H), 8.28 (d, J = 8 Hz, 4H), 8.25 (br.s, 1H), 8.09 (d, J = 2 Hz, 4H), 8.04 (s,1H), 8.01 (s, 4H), 7.82 (s, 2H), 7.69 (d, J = 8 Hz, 1H), 7.00 (d, J = 8 Hz, 1H), 4.03 (t, J = 8 Hz, 2H), 3.45 (t, J = 8 Hz, 2H), 2.00–1.90 (m, 4H), 1.88–1.80 (m, 4H), 1.60–1.50 (m, 40H), -2.72 (brs, 2H); FTIR (neat): *v* 3313, 3095, 2960, 2904, 2865, 2783, 1682, 1592, 1519, 1421, 1247, 973, 799, 717 cm^{-1}; HR mass (MALDI-TOF) calcd. for $C_{81}H_{84}BrN_6O_4$ ([*M*+H]$^+$): 1283.574, found: 1283.574 *m/z*.

Compound **18H$_2$.**

A solution of C_{60} (38.3 mg, 53.2 μmol), **17** (34.2 mg, 26.6 μmol), and *N*-methylglycine (4.74 mg, 53.2 μmol) in toluene (46.0 mL) was refluxed under argon atmosphere in the dark for 15 h. The reaction mixture was allowed to cool to room temperature and then evaporated to dryness at reduced pressure. Flash column chromatography on silica gel with toluene/AcOEt = 20/1 (v/v) as the eluent and reprecipitation from $CHCl_3$-methanol gave **18H$_2$** as a purple solid (17.0 mg, 8.35 μmol, 31% yield). ^{1}H NMR (300 MHz, $CDCl_3$): δ 8.90 (d, J = 5 Hz, 2H), 8.89 (d, J = 5 Hz, 2H), 8.81 (d, J = 5 Hz, 2H), 8.78 (d, J = 5 Hz, 2H), 8.40 (br.s, 1H), 8.36 (d, J = 7 Hz, 2H), 8.27(d, J = 7 Hz, 4H), 8.26 (d, J = 7 Hz, 2H), 8.07 (d, J = 1 Hz, 4H), 8.04 (br.s, 1H), 7.93 (d, J = 9 Hz, 2H), 7.81 (s, 2H), 7.70 (d, J = 8 Hz, 1H), 7.52 (s, 1H), 7.18 (d, J = 8 Hz, 1H), 7.00 (d, J = 8 Hz, 2H), 6.99 (d, J = 8 Hz, 2H), 4.87 (d, J = 8 Hz, 2H), 4.78 (s, 1H), 4.12 (d, J = 8 Hz, 2H), 4.01 (d, J = 7 Hz, 2H), 3.72 (t, J = 7 Hz, 2H), 3.45 (t, J = 7 Hz, 2H), 2.80 (s, 3H), 1.95–1.90 (m, 4H), 1.88–1.80 (m, 4H), 1.60–1.50 (m, 40H), -2.76 (brs, 2H); FTIR (neat): *v* 3308, 2953, 2922, 2859, 2781, 1654, 1593, 1509, 1410, 1244, 799, 719 cm^{-1}; HR mass (MALDI-TOF) calcd. for $C_{143}H_{89}BrN_7O_3$ ([*M*+H]$^+$): 2030.621, found: 2030.623 *m/z*.

Compound **18Zn**.

$Zn(OAc)_2$•$2H_2O$ (18.0mg, 82.0 μmol) was added to a solution of **18H$_2$** (10 mg, 4.90 μmol) in toluene (3.3 mL) and stirred at room temperature overnight. Then, the reaction mixture was filtered and the filtrate was concentrated under reduced pressure. Reprecipitation from $CHCl_3$-methanol gave **18Zn** product as a purple solid (3.5 mg, 1.7 μmol, 34%). ^{1}H NMR (400 MHz, $CDCl_3$/MeOD = 1/1 (v/v)): δ 8.95 (d, J = 5 Hz, 4H), 8.86 (d, J = 5 Hz, 2H), 8.84 (d, J = 5 Hz, 2H), 8.34 – 8.15 (m, 8H), 8.05 (d, J = 6 Hz, 2H), 8.05 (br.s, 1H), 7.95 (d, J = 9 Hz, 2H), 7.80 (s, 2H), 7.67 (d, J = 8 Hz, 1H), 7.67 (s, 1H), 6.98 (d, J = 8 Hz, 2H), 6.97 (d, J = 8 Hz, 2H), 4.65 (d, J = 8 Hz, 2H), 4.50 (s, 1H), 4.01 (d, J = 8 Hz, 2H), 4.00 (d, J = 8 Hz, 2H), 3.44 (t, J = 7 Hz, 2H), 3.43 (t, J = 7 Hz, 2H), 2.72 (s, 3H), 1.95–1.89 (m, 4H), 1.85–1.79 (m, 4H), 1.72–1.65 (m, 8H), 1.60–1.48 (m, 32H).; FTIR (neat): *v* 2952, 1652, 1594, 1510, 1410, 1244, 799, 729 cm^{-1}; HR mass (MALDI-TOF) calcd. for $C_{143}H_{86}BrN_7O_3Zn$ ([*M*]$^+$): 2091.527, found 2091.529 *m/z*

Compound **2**.

A solution of 33 wt.% NMe_3 in ethanol (0.03 mL) was added to a solution of **18Zn** (5.0 mg, 2.6 μmol) in $CHCl_3$ (1.0 mL) under stirring at room temperature and the reaction mixture was kept stirring for 3 days. During the reaction, $CHCl_3$ (1 mL) and the NMe_3 solution (0.03 mL) were added every 24 h. Then, the solution was concentrated under reduced pressure and cyclohexane was added to yield the precipitate. The solid residue was washed with cyclohexane, cyclohexane /CH_2Cl_2 = 1/1 (v/v), then H_2O, followed by drying under a vacuum. The product **2** was obtained as a purple solid (4.4 mg, 2.2 μmol, 80% yield). ^{1}H NMR (500 MHz, DMSO-d_6, 70ºC): δ 10.43 (N*H*CO, brs, 1H), 10.29 (N*H*CO, brs, 1H), 8.85 – 8.65 (m, 9H), 8.40 –8.25 (m, 6H), 8.22–8.15 (m, 2H), 8.02 (brs, 4H) 8.00–7.95 (m, 3H), 7.82 (brs, 2H) 7.81–7.78 (m, 2H), 7.68–7.60 (m, 2H), 7.05–6.95 (m, 2H), 4.69 (brs, 1H), 4.66 (brs, 1H), 4.04 (N^+CH_2, t, J = 6.3 Hz, 2H), 3.91 (brs, 1H), 3.33–3.29 (OCH_2, m, 2H), 3.07 ($N^+(CH_3)_3$, s, 9H), 2.67 (NCH_3, m, 3H), 2.62 (OCH_2CH_2, m, 1H), 2.35 (OCH_2CH_2, m, 1H), 1.83–1.72 (CH_2, m, 4H), 1.55–1.48 (*t*-Bu, m, 30H), 1.45–1.38 (*t*-Bu, m, 6H); FTIR (neat): *v* 3308, 2957, 2867, 1651, 1594, 1509, 1457, 1415, 1315, 1249, 1011, 976, 754, 717 cm^{-1}; HR mass (MALDI-TOF) calcd. for $C_{146}H_{96}N_8O_3Zn$ ([*M*+H-Br]$^+$): 2072.690, found: 2072.690 *m/z*.

Porphyrin-ester **21**.

A solution of **19** (2.11 g, 7.55 mmol) and **20** (3.15 g, 7.53 mmol) in $CHCl_3$ (680 mL) was degassed by bubbling with argon for 10 minutes. The reaction vessel was shielded from ambient light. Then boron trifluoride diethyl etherate (0.945 mL, 7.51 mmol) was added as one portion. The solution was stirred for 2 h at room temperature under argon atmosphere. To the reaction mixture was added *p*-chloranil (3.79 g, 15.4 mmol), and the resulting mixture was stirred for 3 h at room temperature. Then, the reaction was quenched by triethylamine (3.89 mL, 27.9 mmol). For the purification flash column chromatography on alumina with CH_2Cl_2 was first performed. Subsequent flash column chromatography on silica gel with hexane/CH_2Cl_2 = 1/3 to 1/5 (v/v) yielded the desired porphyrin from the mixture. Solvent was removed under reduced pressure and **21** was obtained as a red solid (376 mg, 0.28 mmol, 3.7% yield). m.p. > 300ºC. ^{1}H NMR (400MHz, $CDCl_3$): δ 8.80 (d, *J*=4.9 Hz, 4H), 8.68 (d, *J*=4.9 Hz, 4H), 8.39 (d, *J*=8.3 Hz, 4H), 8.28 (d, *J*=7.8 Hz, 4H), 7.67 (t, *J*=8.5 Hz, 2H), 6.97 (d, *J*=8.3 Hz, 4H), 4.10 (s, 6H), 3.81 (t, *J*=6.3 Hz, 8H), 1.11-0.44 (m, 84H), -2.66 (s, 2H); FTIR (neat): *v* 3321, 2924, 2854, 1728, 1607, 1590, 1457, 1275, 1251, 1101, 967, 799, 762, 735, 632, 548 cm^{-1}; HR mass (MALDI-TOF) calcd. for $C_{88}H_{115}N_4O_8$ ([*M*+H]$^+$) 1355.875, found 1355.872 *m/z*.

Porphyrin-dicarboxylate **22**.

A mixture of **21** (320 mg, 221 μmol) in 160 mL of THF/ethanol = 1/1 (v/v) and potassium hydroxide (1.48 g) in water (17 mL) was refluxed for 8 h. After cooling, the solvent was evaporated, the residue diluted with 300 mL water, and the desired porphyrin dipotassium salt filtered. Acidification (pH 2) of an aqueous suspension of the dipotassium salt with concentrated hydrochloric acid (75 mL) and subsequent filtration gave **22** as a reddish purple solid (291 mg, 313 μmol, 92% yield). m.p. > 300ºC. ^{1}H NMR (400MHz, $CDCl_3$) δ 8.79 (d, *J*=4.9 Hz, 4H), 8.68 (d, *J*=4.9 Hz, 4H), 8.38 (d, *J*=8.3 Hz, 4H), 8.20 (d, *J*=7.8 Hz, 4H), 7.71 (t, *J*=8.3 Hz, 2H), 7.03 (d, *J*=8.8 Hz, 4H), 3.86 (t, *J*=6.1 Hz, 8H), 1.25-0.35 (m, 84H), -2.78 (s, 2H); FTIR (neat): *v* 3317, 2922, 2851, 1692, 1607, 1588, 1456, 1421, 1280, 1248, 1098, 966, 800, 722

cm^{-1}; HR mass (MALDI-TOF) calcd. for $C_{86}H_{111}N_4O_8$ ([*M*+H]$^+$): 1327.840, found 1327.840 *m/z*.

Compound **24**.

A solution of **22** (227 mg, 0.171 mmol), thionyl chloride (3.4 mL), and pyridine (3.4 mL) in dry toluene (35 mL) was refluxed for 4 h under argon atmosphere. The excess reagent and solvents were removed under reduced pressure, and the residue was dissolved in a mixture of dry toluene (55 mL) and pyridine (0.34 mL). To the reaction mixture were added **23** (93.4 mg, 0.205 mmol) and **16** (45.5 mg, 0.220 mmol). The solution was kept stirring for 17 h at room temperature under argon atmosphere. TLC showed three products and the second band was separated by flash column chromatography on silica gel with $CHCl_3$/AcOEt = 10/0 to 10:2 (v/v) as the eluent. The second fraction was concentrated and dissolved in a mixture of $CHCl_3$ (9 mL), trifluoroacetic acid (4.2 mL), and 5 % aqueous sulfuric acid (3 mL). After stirring for 1 d, the reaction mixture was poured onto 50 mL of water and extracted with $CHCl_3$. The organic layer was washed with saturated $NaHCO_3$ aqueous solution (70 mL × 3), dried over anhydrous $MgSO_4$, evaporated, and subsequent flash column chromatography on silica gel (CH_2Cl_2) yielded the desired porphyrin. Compound **24** was obtained as a red solid (29.7 mg, 15.9 μmol, 42 % yield). m.p. > 300ºC. ^{1}H NMR (300 MHz, $CDCl_3$): δ 10.02 (s, 1H), 8.83 (d, *J* = 4.9 Hz, 4H), 8.69 (d, *J* = 12.7 Hz, 4H), 8.30-8.16 (m, 8H), 8.12 (s, 1H), 8.01 (s, 4H), 7.70 (m, 1H), 7.69 (t, *J* = 8.4 Hz, 2H), 7.59 (d, *J* = 8.3 Hz, 1H), 6.99 (d, *J* = 8.3 Hz, 3H), 4.85 (s, 2H), 4.32 (s, 2H), 4.19 (t, *J* = 6.3 Hz, 2H), 4.10 (s, 5H), 3.83 (t, *J* = 6.3 Hz, 8H), 3.48 (t, *J* = 6.6 Hz, 2H), 2.05–1.90 (CH_2, m, 2H), 1.80–1.70 (CH_2, m, 2H), 1.66–1.55 (CH_2, m, 2H), 1.48–1.38 (m, 2H), 1.26–1.22 (m, 4H), 0.94–0.75 (m, 15H), 0.69–0.61 (m, 6H), 0.59–0.46 (m, 20H), 0.41–0.29 (m, 15H), 0.27–0.12 (m, 14H), -2.64 (brs, 2H); FTIR (neat): *v* 3319, 2924, 2853, 1682, 1590, 1522, 1456, 1413, 1319, 1261, 1220, 1165, 1098, 1022, 967, 799, 735 cm^{-1}; HR mass (ESI) calcd. for $C_{115}H_{140}BrFeN_6O_8$ ([*M*+H]$^+$): 1867.926, found 1867.926 *m/z*.

Compound **25H$_2$**.

A solution of C_{60} (7.51 mg, 10.4 μmol), **24** (9.38 mg, 5.02 μmol), and *N*-methylglycine (6.42 mg, 72.1 μmol) in toluene (10 mL) was refluxed under Ar atmosphere in the dark for 20 h. The reaction mixture was allowed to cool to room temperature and then evaporated to dryness at reduced pressure. Flash column chromatography on silica gel with toluene/AcOEt = 50/1 (v/v) as the eluent and reprecipitation from $CHCl_3$-methanol afforded **25H$_2$** as a purple solid (10.4 mg, 3.97 μmol, 79 % yield). ^{1}H NMR (400 MHz, $CDCl_3$): δ 8.81 (d, *J* = 5 Hz, 2H), 8.68 (d, *J* = 5 Hz, 2H), 8.67 (d, *J* = 12 Hz, 4H), 8.35-8.05 (m, 8H), 8.09 (s, 1H), 7.95-7.85 (m, 4H), 7.76 (s, 1H), 7.69 (t, *J* = 8 Hz, 2H), 7.60 (d, *J* = 8 Hz, 1H), 7.07 (d, *J* = 8 Hz, 2H), 6.98 (d, *J* = 8 Hz, 4H), 5.02 (d, *J* = 2 Hz, 1H), 5.01 (s, 1H), 4.84 (m, 2H), 4.32 (m, 2H), 4.30 (d, *J* = 2 Hz, 1H), 4.19 (t, *J* = 6 Hz, 2H), 4.10 (s, 5H), 3.81 (t, *J* = 6 Hz, 8H), 3.48 (t, *J* = 6 Hz, 2H), 2.88 (s, 9H), 2.05–1.93 (CH_2, m, 4H), 1.70–1.60 (CH_2, m, 4H), 1.57–1.55 (CH_2, m, 12H), 1.10–1.00 (m, 8H), 1.00–0.77 (m, 14H), 0.77–0.65 (m, 18H), 0.65–0.50 (m, 15H), 0.50–0.40 (m, 9H), -2.66 (brs, 2H); FTIR (neat): *v* 3319, 2925, 2852, 1681, 1592, 1518, 1457, 1420, 1315, 1248, 1185, 1100, 966, 799, 729 cm^{-1}; HR mass (MALDI-TOF) calcd. for $C_{177}H_{145}BrFeN_7O_7$ ([*M*+H]$^+$): 2614.973, found 2614.977 *m/z*.

Compound **25Zn**.

A saturated methanol solution of $Zn(OAc)_2$•$2H_2O$ (0.5 mL) was added to a solution of **25H$_2$** (10.4 mg, 3.97 μmol) in toluene (3.7 mL) and stirred at room temperature for 1 day. Then, the reaction mixture was filtered and the filtrate was concentrated under reduced pressure. Flash column chromatography on silica gel with toluene/AcOEt = 50/1 (v/v) as the eluent and reprecipitation from $CHCl_3$-methanol gave **25Zn** as a purple solid (10.5 mg, 3.93 μmol, 99 %). ^{1}H NMR (400 MHz, $CDCl_3$): δ 8.82 (d, *J* = 4 Hz, 2H), 8.81 (d, *J* = 4 Hz, 2H), 8.68 (d, *J* = 12 Hz, 4H), 8.30-8.05 (m, 8H), 8.02 (s, 1H), 7.89-7.78 (m, 4H), 7.69 (s, 1H), 7.62 (t, *J* = 8 Hz, 2H), 7.52 (d, *J* = 8 Hz, 1H), 7.17 (d, *J* = 8 Hz, 2H), 7.10 (d, *J* = 8 Hz, 2H), 7.01 (d, *J* = 8 Hz, 2H), 6.92 (d, *J* = 12 Hz, 4H), 4.97 (d, *J* = 2 Hz, 1H), 4.84 (s, 1H), 4.77 (m, 2H), 4.25 (m, 2H), 4.24 (d, *J* = 2 Hz, 1H), 4.11 (t, *J* = 6 Hz, 2H), 4.03 (s, 5H), 3.75 (t, *J* = 6 Hz, 8H), 3.41 (t, *J* = 6 Hz, 2H), 2.81 (s, 9H), 2.00–1.85 (CH_2, m, 4H), 1.60–1.50 (CH_2, m, 4H), 1.48–1.43 (CH_2, m, 12H), 1.30–1.14 (m, 8H), 1.00–0.67 (m, 32H), 0.65–0.50 (m, 15H), 0.50–0.40 (m, 9H); FTIR (neat): *v* 3434, 2924, 2852, 1677, 1604, 1593, 1520, 1455, 1408, 1386, 1248, 1100, 1000, 822, 796, 720 cm^{-1}; HR mass (MALDI-TOF) calcd. for $C_{177}H_{143}BrFeN_7O_7Zn$ ([*M*+H]$^+$) 2676.887, found 2676.885 *m/z*.

Compound **3**.

A solution of 33 wt.% NMe_3 in ethanol (0.03 mL) was added to a solution of **25Zn** (10.0 mg, 3.74 μmol) in $CHCl_3$ (1.0 mL) under stirring at room temperature and the reaction mixture was kept stirring for 3 days. During the reaction, $CHCl_3$ (1mL) and the NMe_3 solution (0.03 mL) were added every 24 h. Then, the solution was concentrated under reduced pressure and cyclohexane was added to yield the precipitate. The solid residue was washed with cyclohexane, cyclohexane /CH_2Cl_2 = 1/1 (v/v), then H_2O, followed by drying under a vacuum. The product **3** was obtained as a purple solid (8.1 mg, 3.3 μmol, 89% yield). ^{1}H NMR (500 MHz, DMSO-d_6, 60ºC): δ 10.52 (N*H*CO, brs, 1H), 10.44 (N*H*CO, brs, 1H), 8.76–8.58 (m, 9H), 8.42 –8.15 (m, 10H), 8.05–7.96 (m, 2H), 7.92–7.85 (m, 2H), 7.78 (brs, 2H), 7.64–7.58 (m, 2H), 7.48–7.42 (m, 2H), 7.12–7.03 (m, 4H), 5.13 (brs, 1H), 5.10 (brd, 1H), 4.87 (Fc, brs, 2H), 4.36 (Fc, brs, 2H), 4.15 (brt, 4H), 4.08 (Fc, brs, 5H), 3.81 (ArOCH_2, m, 8H), 3.36–3.29 (OCH_2, m, 2H), 3.07 (N$^+$(CH_3)$_3$, s, 9H), 2.81 (NCH_3, s, 3H), 2.63 (OCH$_2$CH_2, m, 1H), 2.35 (OCH$_2$CH_2, m, 1H), 2.00–1.92 (CH_2, m, 2H), 1.84–1.72 (CH_2, m, 4H), 1.68–1.59 (CH_2, m, 2H), 1.50–1.45 (m, 2H), 1.30–1.20 (m, 4H), 0.97–0.79 (m, 26H), 0.74–0.65 (m, 6H), 0.61–0.47 (m, 32H), 0.45–0.37 (m, 6H); FTIR (film): *v* 3293, 3099, 2924, 2853, 2784, 1668, 1605, 1521, 1455, 1411, 1321, 1249, 1199, 996, 820, 794, 718 cm^{-1}; HR mass (MALDI-TOF) calcd. for $C_{180}H_{152}FeN_8O_7Zn$ ([*M*+H-Br]$^+$): 2658.042, found 2658.039 *m/z*.

Theoretical calculations:

Geometries were optimized using the Gaussian 09 Revision D.01 program[7] with the B3LYP[8] functional with the D3 version of Grimme's dispersion with the original D3 damping function[9]. The 6-31G(d)[10] basis set was used for H, C, N and O atoms, and Los Alamos ECP plus DZ[11] was used for Fe and Zn atoms. On the calculation for **3**, the all decyl chains were substituted by propyl chains based on the theoretical experimental facts that they are sufficient for demonstrating the substituent effect. For single point calculations, the 6-311G(d) basis set[12] was used with diffuse functions[13] on N atoms. The basis set superposition errors, BSSE, were evaluated with the counterpoise method.[14] Solvent effects have been included for several calculations by means of the PCM method.[15]

Atomic force microscopy:

Atomic force microscopy images were obtained with a MFP-3D-SA atomic force microscope (Asylum Technology) in an AC mode. AC240TS microcantilevers (Olympus), which have a force constant of 1.7 N m^{-1} and a nominal tip radius of less than 10 nm, were used for all measurements. The sample was deposited onto a cleaved mica substrate by precipitation from a solution droplet, followed by washing with water, and then dried with N_2 blowing. All measurements were performed in air. Size of the particles was evaluated as follows. Acquired images were analyzed by Image J[16] with a function of "analyze particle" on 16-bit monochrome image to determine a mean height and an area of the particles. Then, the size of the particles, which deemed as a sphere, was calculated from the volume of the particles.

Nanosecond transient absorption measurements:

Nanosecond time-resolved TA measurements were carried out using the laser system (UNISOKU Co., Ltd., Osaka, Japan). Solvents were deaerated by argon purging for 5-60 min prior to measurements. A solution containing the compound was excited by a Panther OPO pumped by a Nd:YAG laser (Continuum SLII-10, 4-6 ns fwhm), and the photodynamics were monitored by continuous exposure to a Xenon lamp (150 W) as a probe light and a photomultiplier tube (Hamamatsu 2949) as a detector.

Evaluation on the relative charge-separation yield (Φ_{calcd}):

Φ_{calcd} in Tables 3 and S2 was determined by the recorded nanosecond TA spectra and the following equation:[17]

$$\Phi_{calcd} = \Phi_{ref} \times \frac{\Delta OD_{max\text{-}sample}}{\Delta OD_{max\text{-}ref}}$$

where Φ_{ref} is the CS yield of the reference compound (0.99 for **5** in PhCN)[17], $\Delta OD_{max\text{-}sample}$ and $\Delta OD_{max\text{-}ref}$ are the maximum ΔOD intensities at 1000 nm of the compound of interest and the reference compound (**5** in the present case). Difference of the molar extinction coefficients and the influence of the aggregation in the solvent systems are taken into account with the data of the fullerene radical anion obtained in this study (Table S4) by using the literature procedure.[18] $\Delta OD_{max\text{-}sample}$ and $\Delta OD_{max\text{-}ref}$ must be recorded by using the same apparatus under the same experimental conditions, i.e. excitation wavelength and power, laser pulse, absorption of a sample at the wavelength, recording time scale and resolution, and temperature.

Fluorescence lifetime measurements:

The instruments used were described elsewhere.[19] In brief, Ti:sapphire laser pumped by CW Nd laser was used to generate 50 fs at 820 nm. The second harmonic was used to excite the sample, the sample emission was mixed with the laser fundamental harmonic and the signal at sum frequency was passed through a color filter and monochromator and detected by a photomultiplier working in a single photon counting mode with a time-correlated single photon counting (TCSPC) method. The time resolution was ~80 ps (fwhm). An up-conversion technique for fluorescence was used to detect the fast processes. The

time resolution of the instrument was 150-200 fs (FWHM).

PC12 Cell culture:

Rat pheochromocytoma (PC12) cells were cultured in Dulbecco's modified Eagle's minimal essential medium (DMEM) with high glucose (SIGMA-ALDRICH) supplemented with 5% Fetal bovine serum (FBS) (Japan Bioserum, Hiroshima, Japan) and 5% horse serum (HS) (Thermo Fisher Scientific Inc., MA, USA). The cell culture media contained 30 U/mL penicillin and 30 μg/mL streptomycin (Thermo). The cells were cultured in 5% CO_2 and 95% air, and were passaged every 3–4 days. PC12 cells were used for the following experiments with this culturing condition unless stated.

Confocal microscopy:

PC12 cells were cultured on poly-L-lysine (PLL) coated glass bottom dish. After 1 day, medium was removed, washed once with HBSS(+) and filled with HBSS(+). Then, an aqueous solution of the compound was added to the cells to adjust the final concentration of 0.6 μM based on the compound. The cells were incubated for 3 min and washed by HBSS once and filled by HBSS(+). Confocal images were recorded by Zeiss LSM780 (Carl Zeiss Microscopy GmbH, Jena, Germany), which equips a 40 oil objective lens (NA 0.75), GaAsP (32x) array and fs–pumped pulsed laser. An image of the compound was obtained by using spectral imaging with liner unmixing.

Incorporation of the compounds into liposome:

To aqueous solution of COATSOME® EL-11-A (Lipid composition: POPC:Cholesterol:POPG = 30:40:30 mol%) (NOF Co., Tokyo, Japan), 1.00 mM DMSO solution of **1**, **2** or **3** was added at a concentration of 1 mol% relative to the lipids and incubated at 37˚C, where the concentration of DMSO is less 1 vol% relative to H_2O. The incorporation was monitored by following the change in the absorbance of the Soret band. Typically, it was completed within one hour.[1]

Detection of photo-induced reactive oxygen species (ROS):

Detection of ROS with Singlet Oxygen Sensor Green Reagent (for $^1O_2$) (Thermo Fisher Scientific Inc., MA, USA) or MPEC® (for O_2^-) (ATTO, Tokyo, Japan) was performed on the basis of the manufacture's protocol. Briefly, 1.0 μM of the compound containing 5.0 μM SOSGR or 5.0 μM MPEC in deionized H_2O containing 1.0% DMSO was irradiated in a cuvette for 2 min by Xe lamp (2.0 mW cm^{-2}) with a band-pass filter (400-450 nm). The resulting solutions were immediately subjected to the spectrofluorometer with excitation wavelength at 490 nm (for $^1O_2$) or Lumat LB 9507 luminometer (Berthold Tech, Canada.) (for O_2^-). The measurements were repeated for three times at least and the results were statistically processed.

Detection of photoinduced cell damage:

Detection of cell necrosis/apoptosis was carried out by using Annexin V-FITC Apoptosis Kit (BioVision, Inc., CA, USA), which contains Annexin V-FITC conjugate for early apoptosis detection and propidium iodide (PI) for late apoptosis and necrosis detection, according to the manufacture's protocol. Briefly, the cells were seeded at (PLL) coated glass bottom dish with 1.0×10^5 cells mL^{-1} and cultured for 1 day.

Then, the medium was removed, washed with HBSS(-) twice and filled with HBSS(-). Then, an aqueous solution of the compound was added to the cells to the final concentration of 0.6 μM based on the compound. The cells were incubated for 3 min at room temperature and washed by HBSS(-) once and filled by HBSS(-), followed by the illumination of the Xe lamp (2.0 mW cm^{-2}, 400-450 nm) for 2 min. After the irradiation, the cells were treated by the Annexin V-FITC/PI solution, then observed by a Fluoview-10i (Olympus). Fluorescent cells were counted as cells in early apoptosis (green) or those in late apoptosis or necrosis (red or yellow). For one experiment, more than 500 cells were counted from randomly chosen three images (more than 150 cells per an image). Assays were performed in triplicate and the results were analyzed statistically.

Evaluation on the numbers of incorporated molecules in a single cell:

PC12 cells (8×10^5 cells) were seeded on a six-well plate (Corning, MA, USA) and cultured for 24±3 hrs. After removing the medium, the cells were washed twice with HBSS(-), and filled with HBSS(-). Then, an aqueous solution of the compound was added to the cells to adjust the final concentration of 0.60 μM based on the compound. The cells were incubated for 3 min and washed by PBS(-) and dissolved by 0.2 % TritonX-100 aq. and dried in a vacuum. The residue was extracted by DMSO and the extract was subjected to the absorption spectrometer. The total number of the molecules was obtained by the relative integration value of the Soret band intensity to the reference (2.00 μM DMSO solution of the corresponding compound). Then, the number was divided by the number of the cells which were treated similarly by HBSS(-) instead of the aqueous solution of the compound.

Rat hippocampal neuron culture:

Primary cultures of hippocampal neurons were prepared as previously described with slight modifications.[20] In brief, hippocampi were dissected from embryonic day 17 (E17) or E18 rats. Hippocampal neurons were dissociated by using SUMITOMO Nerve-Cell Culture System (Sumitomo Bakelite, Tokyo, Japan) and plated on coverslips coated with poly-D-lysine (SIGMA-Aldrich) at a density of 4.5×10^4 cells/cm^2 in MEM supplemented with 10% horse serum (Life Technologies, CA, USA), 0.6% D-glucose, 1 mM sodium pyruvate, 100 U/mL penicillin and 100 μg/mL streptomycin. Three hours after plating, media was replaced by Neurobasal medium (Life Technologies) supplemented with 2% B-27 supplement (Life Technologies), 0.5 mM L-glutamine (SIGMA-Aldrich), 100 U/mL penicillin and 100 μg/mL streptomycin. All neurons were maintained at 37 ˚C in 5% CO_2 in a humidified incubator before being used for patch-clamp experiments.

Patch clamp measurements:

Whole-cell patch recordings for current clamp were recorded using nystatin-perforated patch technique on PC12 cells and rat hippocampal neurons at room temperature (22–25 °C) with Axopatch 200B patch-clamp amplifier (Molecular Devices, CA, USA). An aqueous solution of the compound was added to the cells to adjust the final concentration of 0.6 μM based on the compound. For the whole-cell recordings, the Na^+–based bath solution contained (in mM) 140 NaCl, 5 KCl, 2 $CaCl_2$, 1 $MgCl_2$, 10 HEPES, and 10 *D*-glucose (pH adjusted to 7.40 with NaOH, and osmolality adjusted to 320

mosmol/kgH_2O with *D*-mannitol). The pipette solution contained (in mM) 55 K_2SO_4, 20 KCl, 5 $MgCl_2$, 0.2 EGTA, and 5 HEPES (pH adjusted to 7.40 with KOH, and osmolality adjusted to 300 mosmol/kgH_2O with *D*-mannitol). Photo-induced V_m was calculated by the following equation; V_m (mV) = $V_{hv} - V_{Ctl}$ where V_{hv} and V_{Ctl} are membrane potentials observed after and before illumination (Ultra high pressure Hg lamp, 2.0 mW cm^{-2}, 400-450 nm).

Planner patch clamp measurements with illumination of NIR laser:

To PC12 cells which were grown to 70% confluence, Dispase (2.0 CU/mL) (Corning Inc., MA, USA) was added, followed by incubation for 6–12 h at 37°C. Suspended cells were transfer to a new dish with using a 0.4 μm strainer, washed by HBSS(+) twice and collected as suspension in HBSS(+) and used for planner patch recordings. Whole-cell patch mode for current clamp was recorded using escin-perforated patch technique on PC12 cells at room temperature (22-25 °C) with EPC-10 USB patch-clamp amplifier (HEKA Elektronik Dr. Schulze GmbH, Germany) combined with a Port–a–Patch® (Nanion Technologies, Munich, Germany). An aqueous solution of the compound was added to the cells to adjust the final concentration of 0.6 μM based on the compound. For whole-cell recordings, the Na^+–based bath solution contained (in mM) 140 NaCl, 4 KCl, 2 $CaCl_2$, 1 $MgCl_2$, 10 HEPES, and 5 *D*-glucose (pH adjusted to 7.40 with NaOH, and osmolality adjusted to 298 mosmol/kgH_2O with *D*-mannitol). The pipette solution contained (in mM) 10 NaCl, 50 KCl, 60 KF, 20 EGTA, and 10 HEPES (pH adjusted to 7.20 with KOH, and osmolality adjusted to 285 mosmol/kgH_2O with *D*-mannitol). For ensuring sufficient seals, the data were only collected from the cells that demonstrated seal resistance value more than 1 GΩ after the perforation (56% success rate where n = 30). Xe lamp with a band-pass filter (2 mW cm^{-2} (0.1 μW on a cell), 400–450 nm) or fs–pumped pulsed laser (Chameleon-RF, COHERENT) (250 mW cm^{-2} (6 μW on a cell), 860 nm) was used as a light source.

References:

1. T. Numata, T. Murakami, F. Kawashima, N. Morone, J. E. Heuser, Y. Takano, K. Ohkubo, S. Fukuzumi, Y. Mori and H. Imahori, *J. Am. Chem. Soc.*, 2012, **134**, 6092-6095.
2. H. Imahori, K. Tamaki, H. Yamada, K. Yamada, Y. Sakata, Y. Nishimura, I. Yamazaki, M. Fujitsuka and O. Ito, *Carbon*, 2000, **38**, 1599-1605.
3. N. Topnani, V. Hamplova, M. Kaspar, V. Novotna and E. Gorecka, *Liq. Cryst.*, 2014, **41**, 91-100.
4. H. Imahori, T. Azuma, A. Ajavakom, H. Norieda, H. Yamada and Y. Sakata, *J. Phys. Chem. B*, 1999, **103**, 7233-7237.
5. J. W. Ka and C. H. Lee, *Tetrahedron Lett.*, 2000, **41**, 4609-4613.
6. M. Yamamoto, Y. Takano, Y. Matano, K. Stranius, N. V. Tkachenko, H. Lemmetyinen and H. Imahori, *J. Phys. Chem. C*, 2014, **118**, 1808-1820.
7. Frisch, M. J., Trucks, G. W., Schlegel, H. B., Scuseria, G. E., Robb, M. A., Cheeseman, J. R., Scalmani, G., Barone, V., Mennucci, B., Petersson, G. A., Nakatsuji, H., Caricato, M., Li, X., Hratchian, H. P., Izmaylov, A. F., Bloino, J., Zheng, G., Sonnenberg, J. L., Hada, M., Ehara, M., Toyota, K., Fukuda, R.; Hasegawa, J.; Ishida, M.; Nakajima, T.; Honda, Y.; Kitao, O.; Nakai, H.; Vreven, T.; Montgomery, Jr., J. A.; Peralta, J. E.; Ogliaro, F.; Bearpark, M.; Heyd, J. J.; Brothers, E.;

Kudin, K. N.; Staroverov, V. N.; Kobayashi, R.; Normand, J.; Raghavachari, K.; Rendell, A.; Burant, J. C.; Iyengar, S. S.; Tomasi, J.; Cossi, M.; Rega, N.; Millam, J. M.; Klene, M.; Knox, J. E.; Cross, J. B.; Bakken, V.; Adamo, C.; Jaramillo, J.; Gomperts, R.; Stratmann, R. E.; Yazyev, O.; Austin, A. J.; Cammi, R.; Pomelli, C. J.; Ochterski, W.; Martin, R. L.; Morokuma, K.; Zakrzewski, V. G.; Voth, G. A.; Salvador, P.; Dannenberg, J. J.; Dapprich, S.; Daniels, A. D.; Farkas, O.; Foresman, J. B.; Ortiz, J. V.; Cioslowski, J. and Fox, D. J. GAUSSIAN 09, Revision A.02; Gaussian, Inc., Wallingford CT, (2009).

8. (a) A. D. Becke, *Phys. Rev. A*, 1988, **38**, 3098-3100. (b) A. D. Becke, *J. Chem. Phys.*, 1993, **98**, 5648-5652. (c) C. T. Lee, W. T. Yang and R. G. Parr, *Phys. Rev. B*, 1988, **37**, 785-789. (d) M. M. Francl, W. J. Pietro, W. J. Hehre, J. S. Binkley, M. S. Gordon, D. J. Defrees and J. A. Pople, *J. Chem. Phys.*, 1982, **77**, 3654-3665.
9. S. Grimme, J. Antony, S. Ehrlich and H. Krieg, *J. Chem. Phys.*, 2010, **132**, 154104.
10. (a) G. A. Petersson and M. A. Allaham, *J. Chem. Phys.*, 1991, **94**, 6081-6090. (b) G. A. Petersson, A. Bennett, T. G. Tensfeldt, M. A. Allaham, W. A. Shirley and J. Mantzaris, *J. Chem. Phys.*, 1988, **89**, 2193-2218.
11. P. J. Hay and W. R. Wadt, *J. Chem. Phys.*, 1985, **82**, 299-310.
12. (a) A. D. Mclean and G. S. Chandler, *J. Chem. Phys.*, 1980, **72**, 5639-5648. (b) R. Krishnan, J. S. Binkley, R. Seeger and J. A. Pople, *J. Chem. Phys.*, 1980, **72**, 650-654.
13. T. Clark, J. Chandrasekhar, G. W. Spitznagel and P. V. Schleyer, *J. Comput. Chem.*, 1983, **4**, 294-301.
14. S. Simon, M. Duran and J. J. Dannenberg, *J. Chem. Phys.*, 1996, **105**, 11024-11031.
15. M. Cossi, G. Scalmani, N. Rega and V. Barone, *J. Chem. Phys.*, 2002, **117**, 43-54.
16. C. A. Schneider, W. S. Rasband and K. W. Eliceiri, *Nat. Methods*, 2012, **9**, 671-675.
17. H. Imahori, K. Tamaki, D. M. Guldi, C. P. Luo, M. Fujitsuka, O. Ito, Y. Sakata and S. Fukuzumi, *J. Am. Chem. Soc.*, 2001, **123**, 2607-2617.
18. C. P. Luo, M. Fujitsuka, C. H. Huang and O. Ito, *Phys. Chem. Chem. Phys.*, 1999, **1**, 2923-2928.
19. N. V. Tkachenko, L. Rantala, A. Y. Tauber, J. Helaja, P. H. Hynninen and H. Lemmetyinen, *J. Am. Chem. Soc.*, 1999, **121**, 9378-9387.
20. K. Goslin, H. Asmussen and G. Banker, *In Culturing Nerve Cells*, ed. G. Banker and K. Goslin, The MIT Press, Cambridge, MA, 1998, Rat hippocampal neurons in low-density culture. 339–370.
21. *Recommended Reference Materials for the Realization of Physicochemical Properties*; K. N. Marsh, ed. Blackwell Scientific Publications: Oxford, U.K., 1987.
22. J. F. Lou, T. A. Hatton and P. E. Laibinis, *J. Phys. Chem. A*, 1997, **101**, 5262-5268.
23. S. Fukuzumi, H. Kotani, K. Ohkubo, S. Ogo, N. V. Tkachenko and H. Lemmetyinen, *J. Am. Chem. Soc.*, 2004, **126**, 1600-1601
24. C. P. Luo, M. Fujitsuka, C. H. Huang and O. Ito, *Phys Chem. Chem. Phys.*, 1999, **1**, 2923-2928.

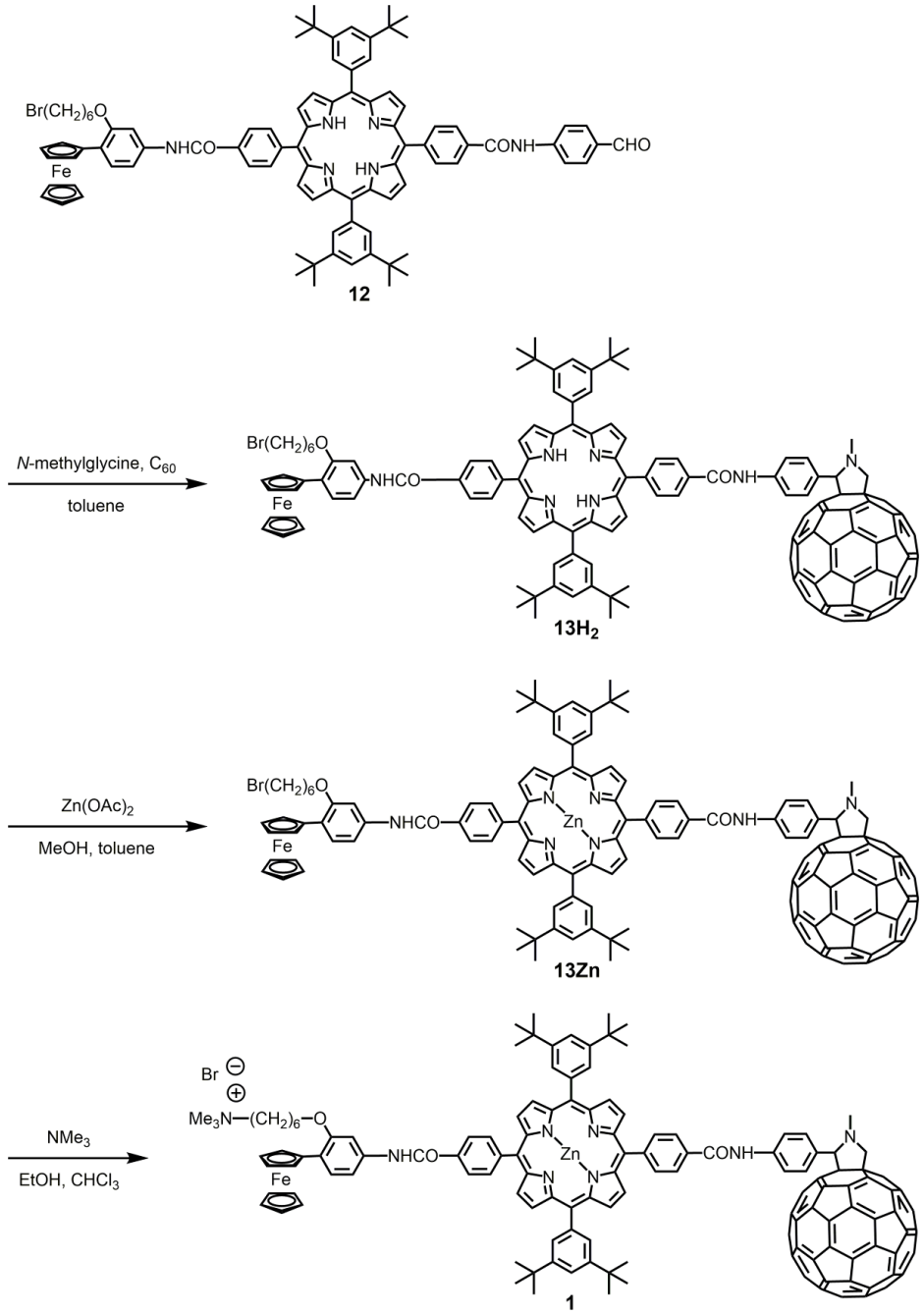

Fig. S1 Synthetic scheme for **1**.

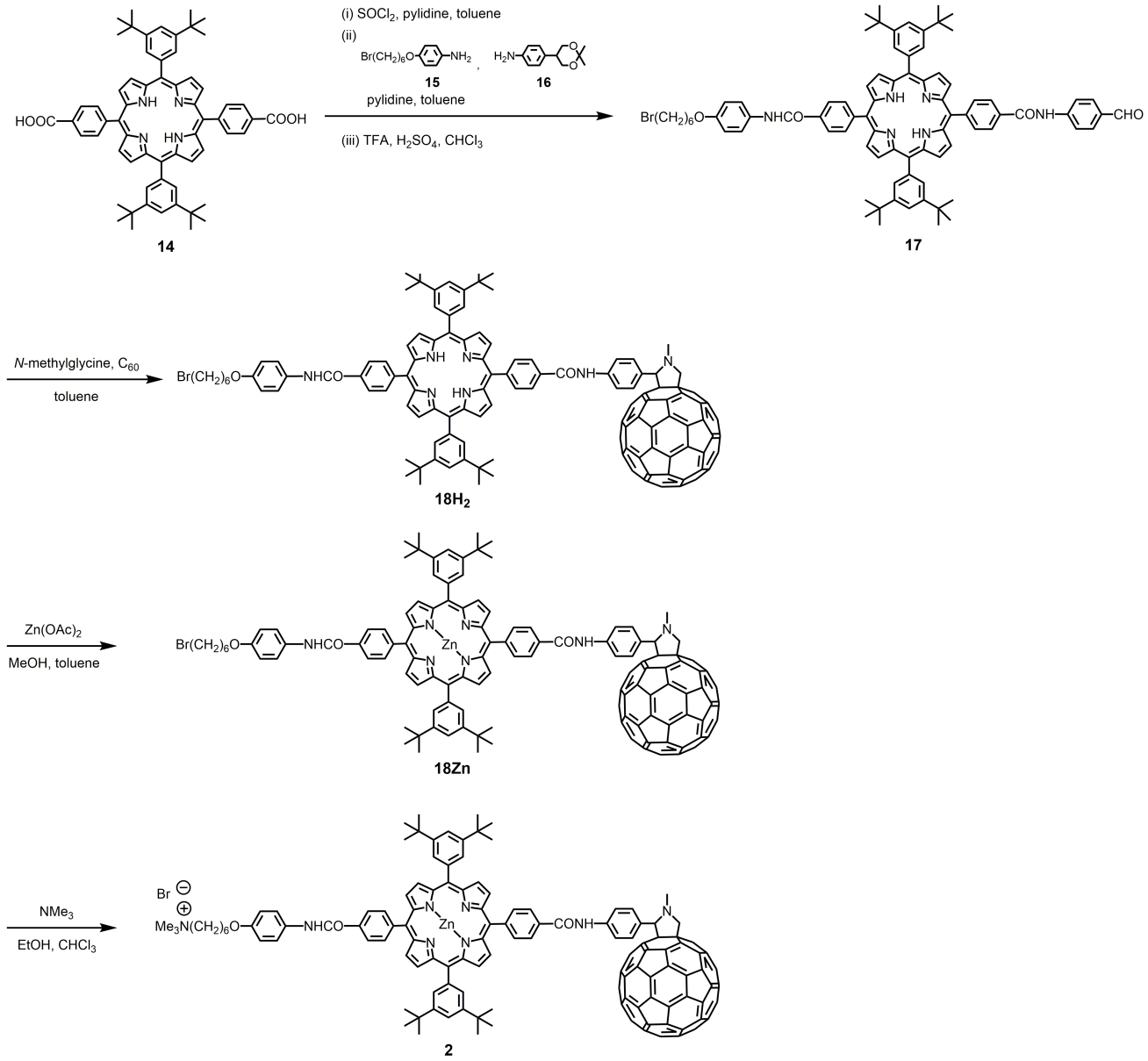

Fig. S2 Synthetic scheme for **2**.

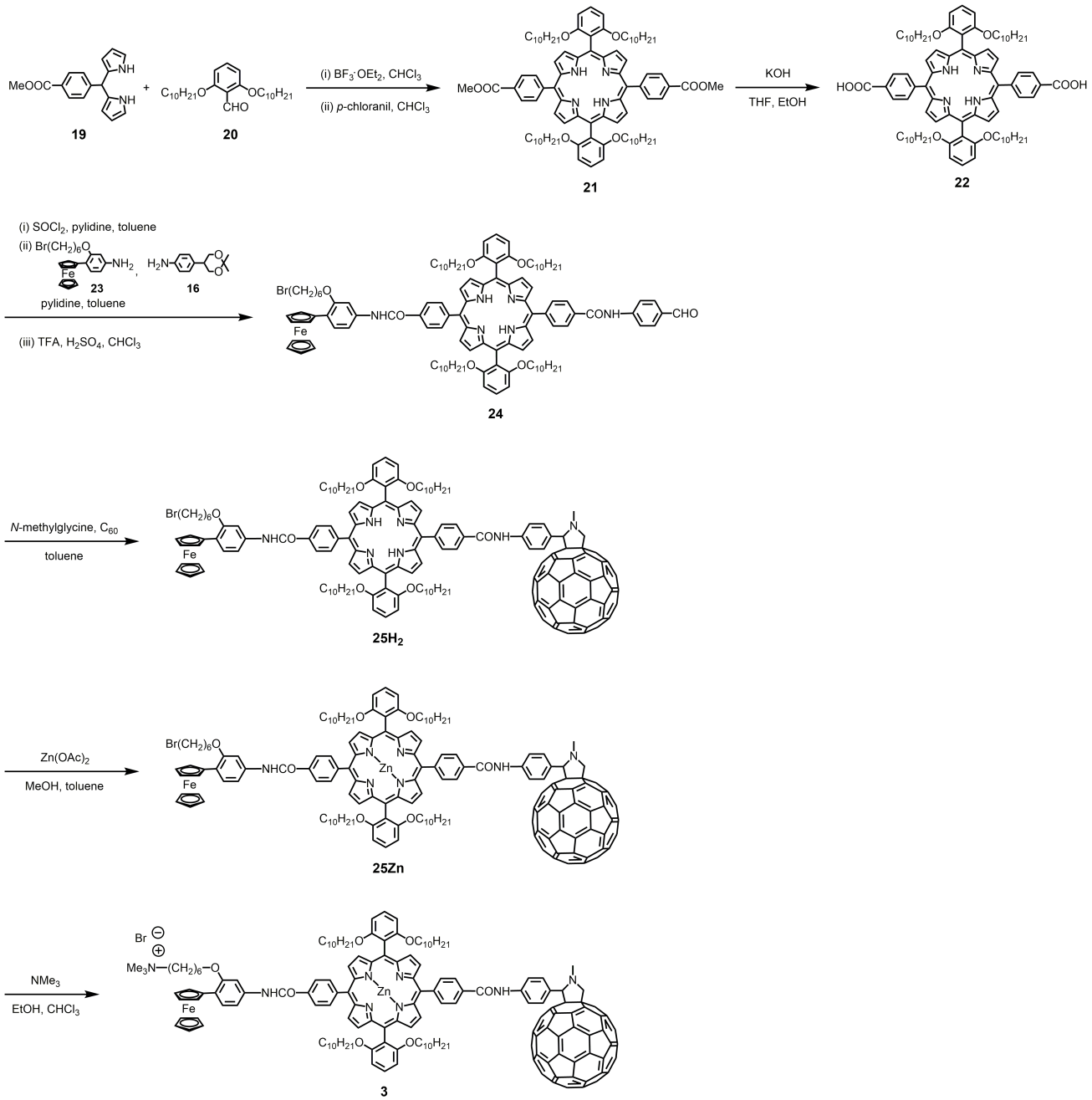

Fig. S3 Synthetic scheme for **3**.

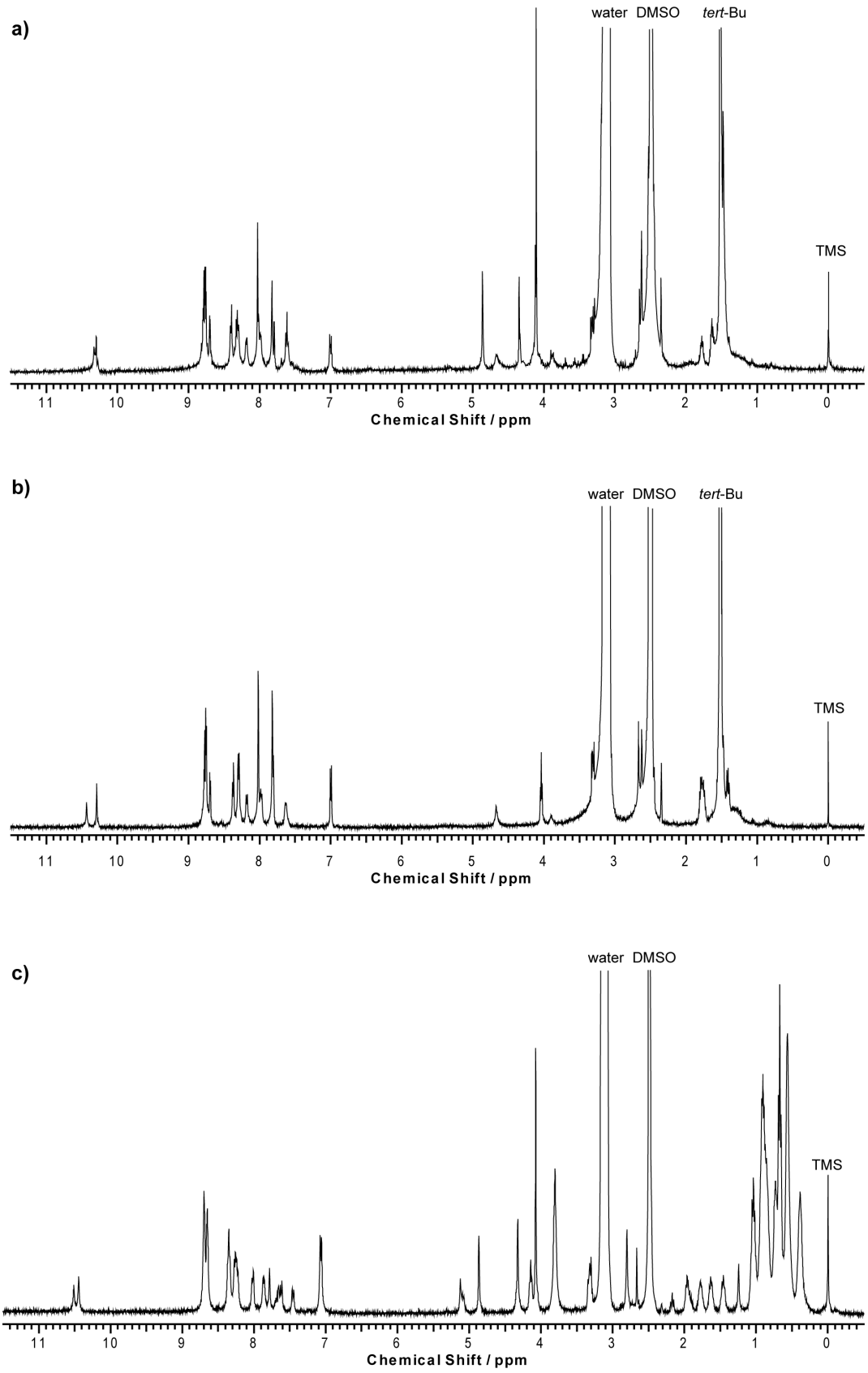

Fig. S4 ^{1}H NMR spectra of (a) **1** at 70˚C, (b) **2** at 70˚C and (c) **3** at 60˚C in DMSO-d_6.

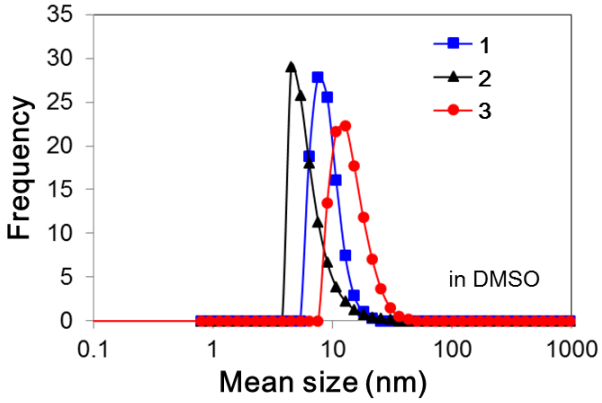

Fig. S5 Particle number-based size distributions of **1**-**3** in DMSO measured by DLS.

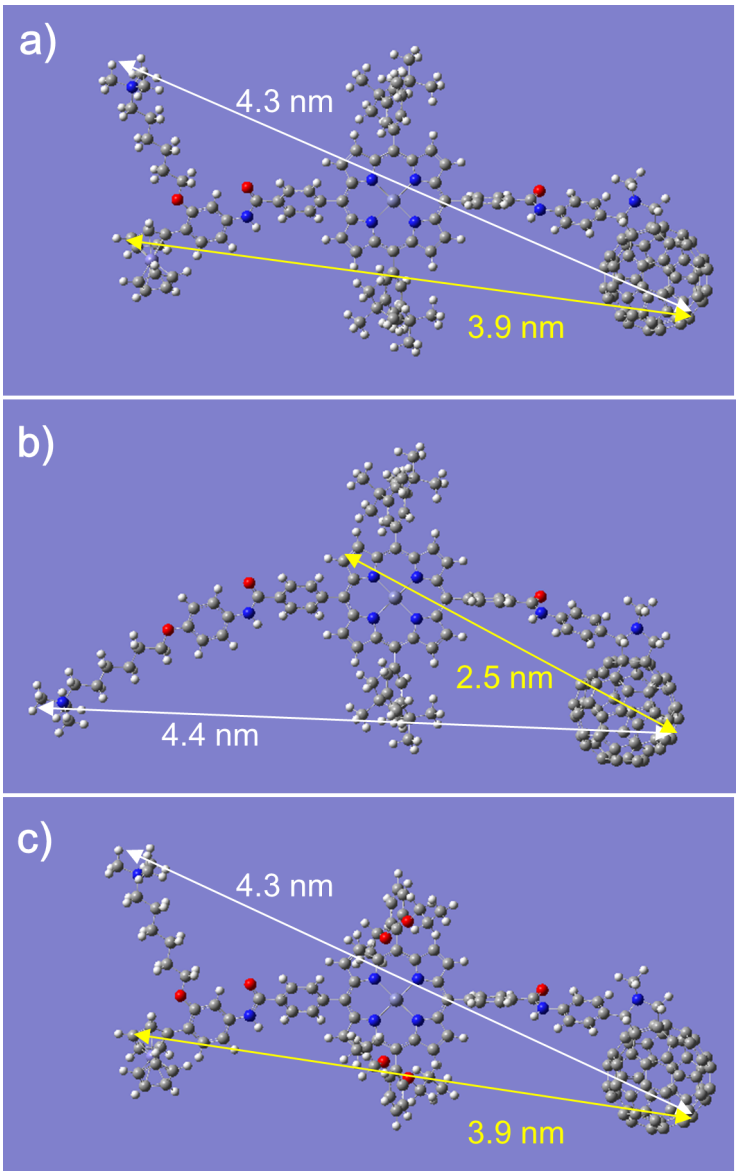

Fig. S6 DFT optimized structures of (a) **1**, (b) **2** and (c) **3**, where Br anion has been removed to simplify the calculations at the UB3LYP-D3/6-31G(d) [C, H, N, O], LANL2DZ [Fe, Zn] level of theory. Embedded white allows and values in nm unit denote the separation distances between the most distant pair of atoms, and the yellow allows and values denote the edge-to-edge distance of the corresponding ion pairs. Taking into account the van der Waals radius, the molecular lengths of **1-3** are ca. 5 nm.

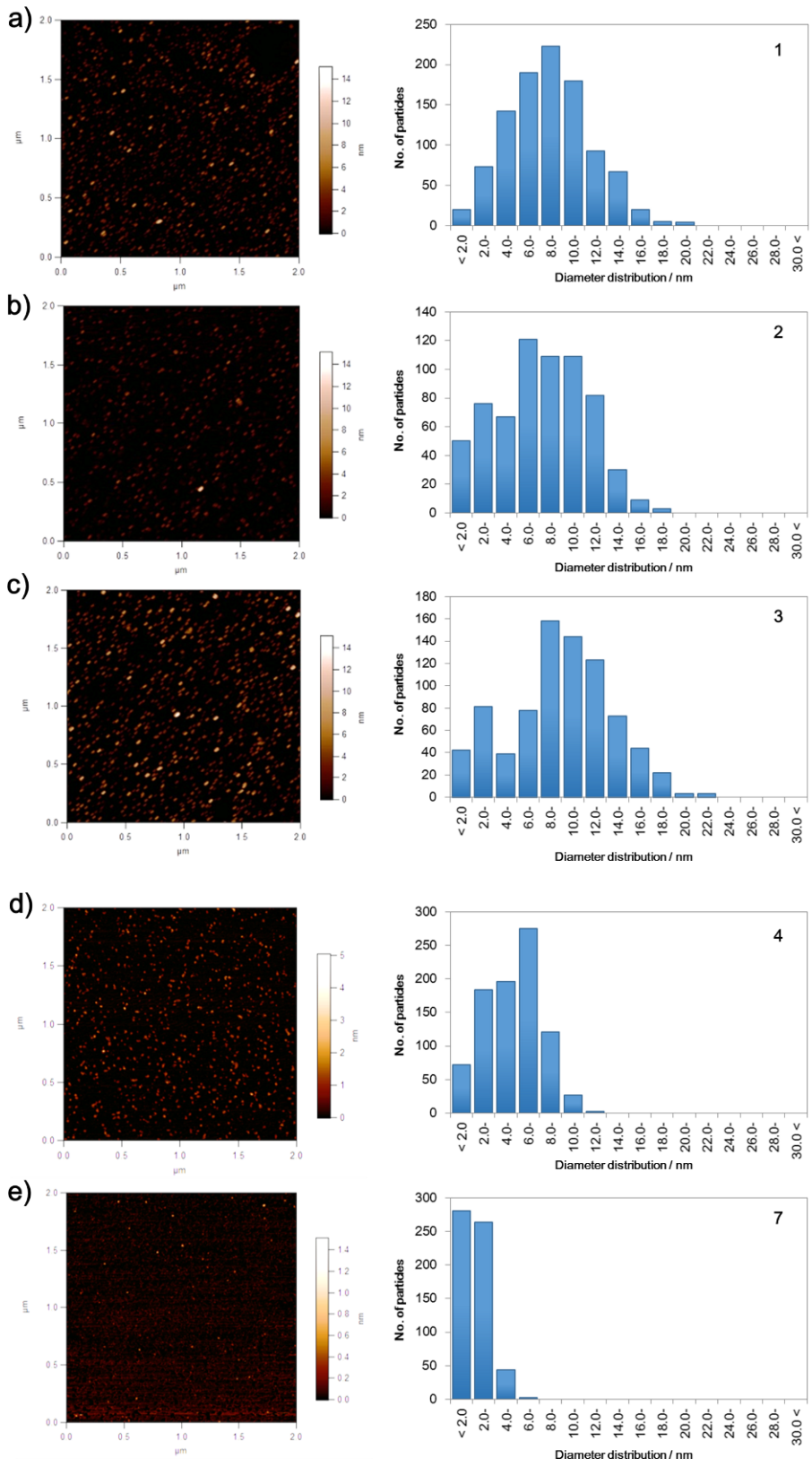

Fig. S7 AFM images (left) and histograms of the size distribution (right) of (a) **1**, (b) **2**, (c) **3**, (d) **4** and (e) **7**.

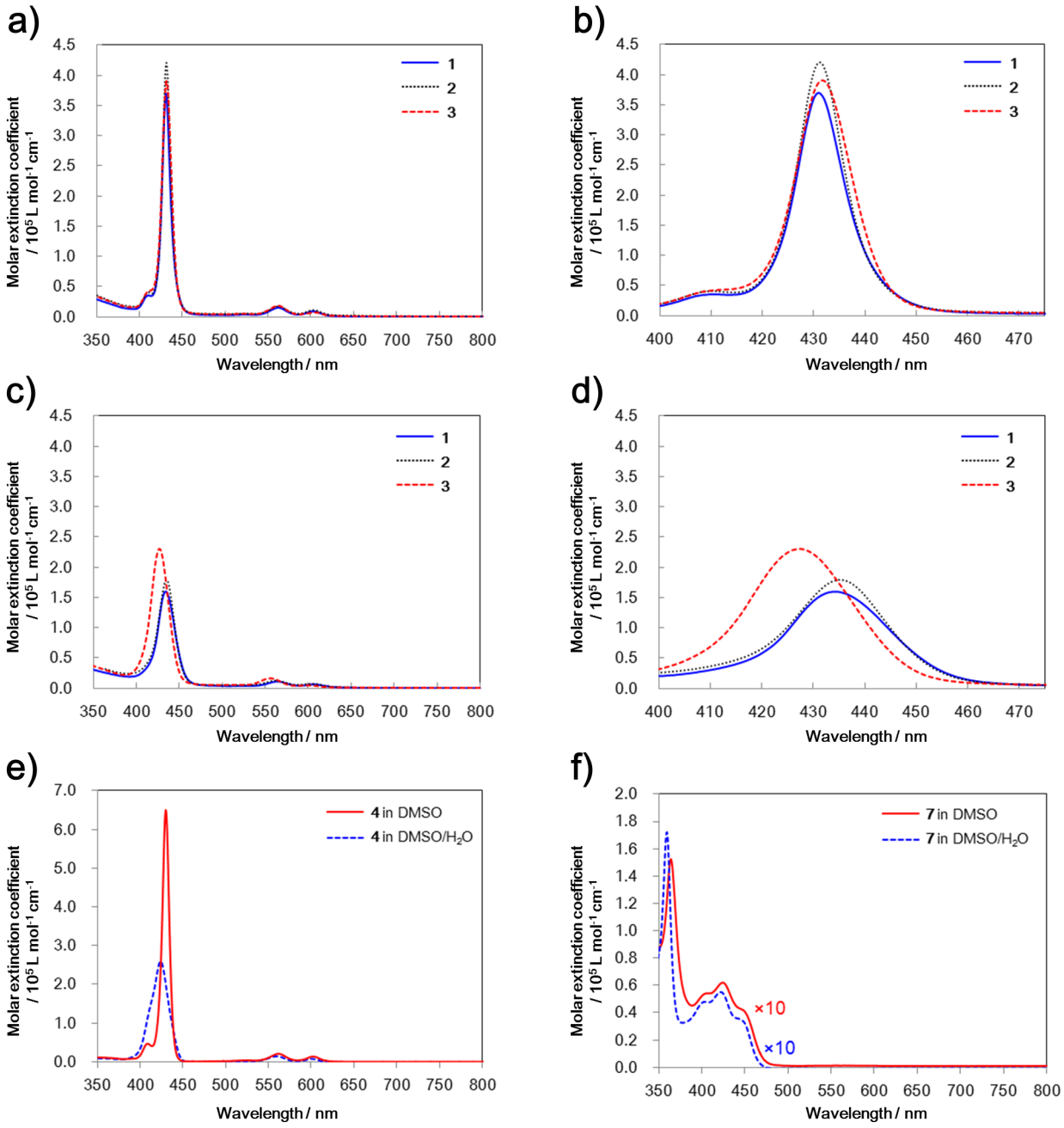

Fig. S8 UV-visible absorption spectra of (a) **1**-**3** in DMSO, (c) **1**-**3** in DMSO/H_2O (1:99, v/v), (e) **4** in DMSO and DMSO/H_2O (1:99, v/v), and (f) **7** in DMSO and DMSO/H_2O (1:99, v/v). Expanded spectra in the region of the Soret band of (b) **1**-**3** in DMSO and (d) **1**-**3** in DMSO/H_2O (1:99, v/v).

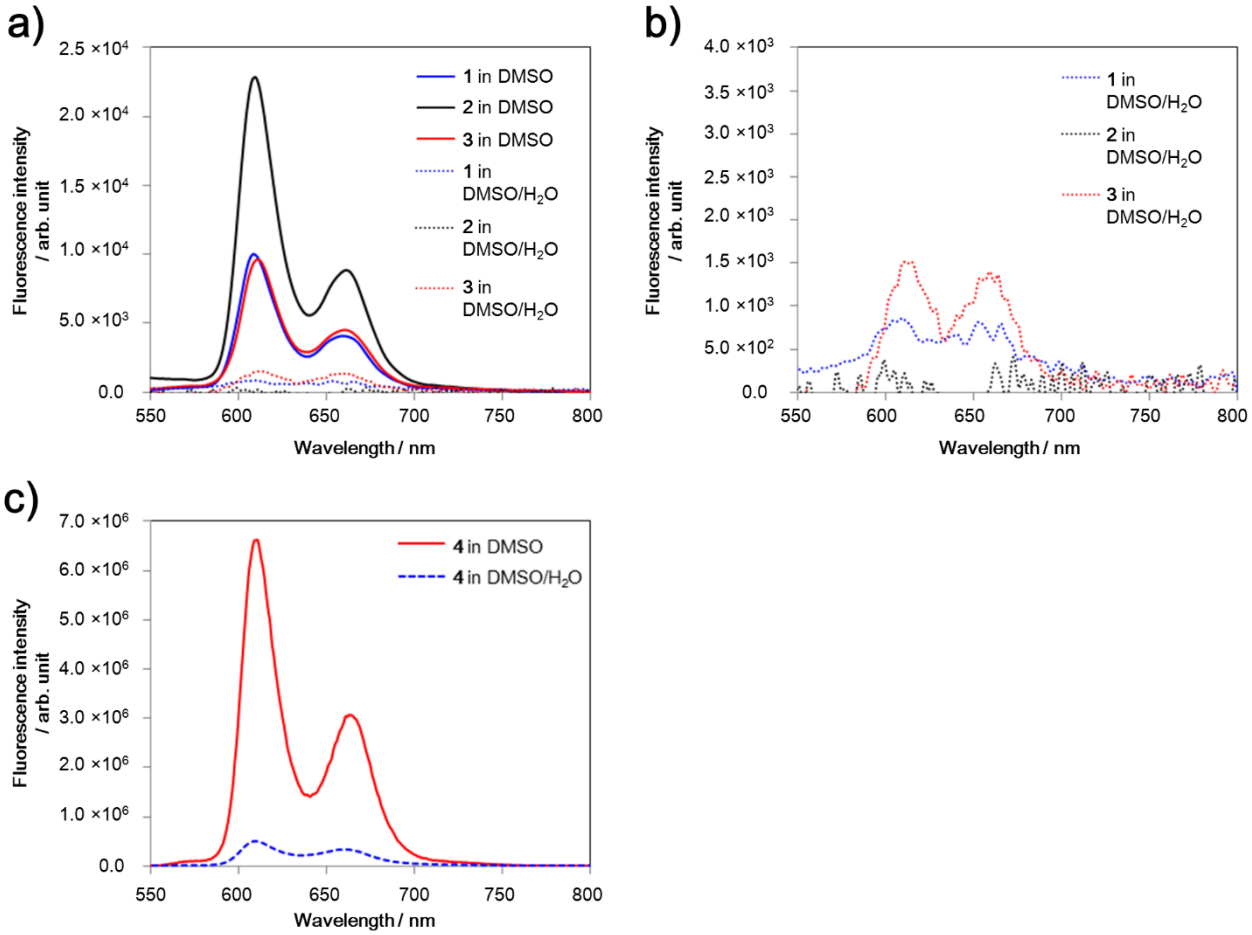

Fig. S9 (a) Fluorescence spectra of **1**-**3** in DMSO (solid line) and DMSO/H_2O (1:99, v/v) (dotted line). (b) Magnified fluorescence spectra of **1**-**3** in DMSO/H_2O (1:99, v/v). (c) Fluorescence spectra of **4** in DMSO and DMSO/H_2O (1:99, v/v). The fluorescence spectra were obtained by the excitation at Soret band where the absorbances were adjusted to be identical (0.30).

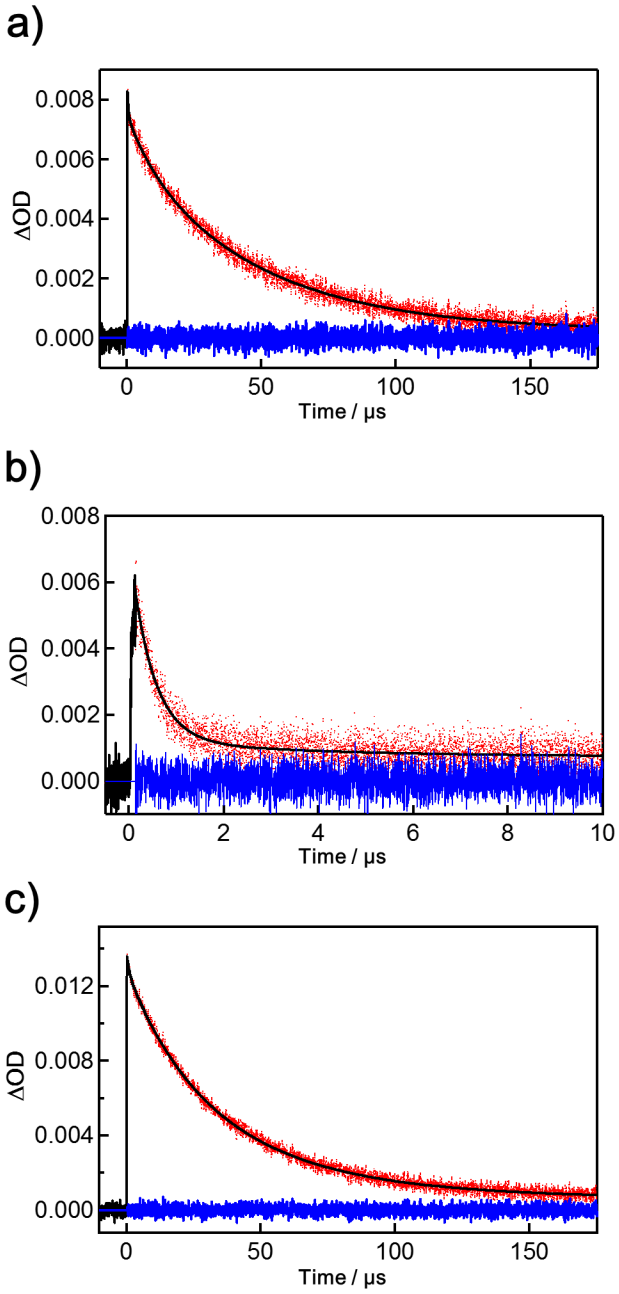

Fig. S10 Decay time profiles of (a) **1**, (b) **2** and (c) **3** at 1000 nm arising from $C_{60}^{\bullet-}$, which were obtained by nanosecond time-resolved TA measurements in deaerated DMSO after nanosecond laser excitation. The profiles were obtained by the excitation at 410 nm where the absorbances were adjusted to be identical (0.50). Red plots are the observed signals, black line is drawn by the single-exponential or bi-exponential fitting, and blue line is the residual after the fitting.

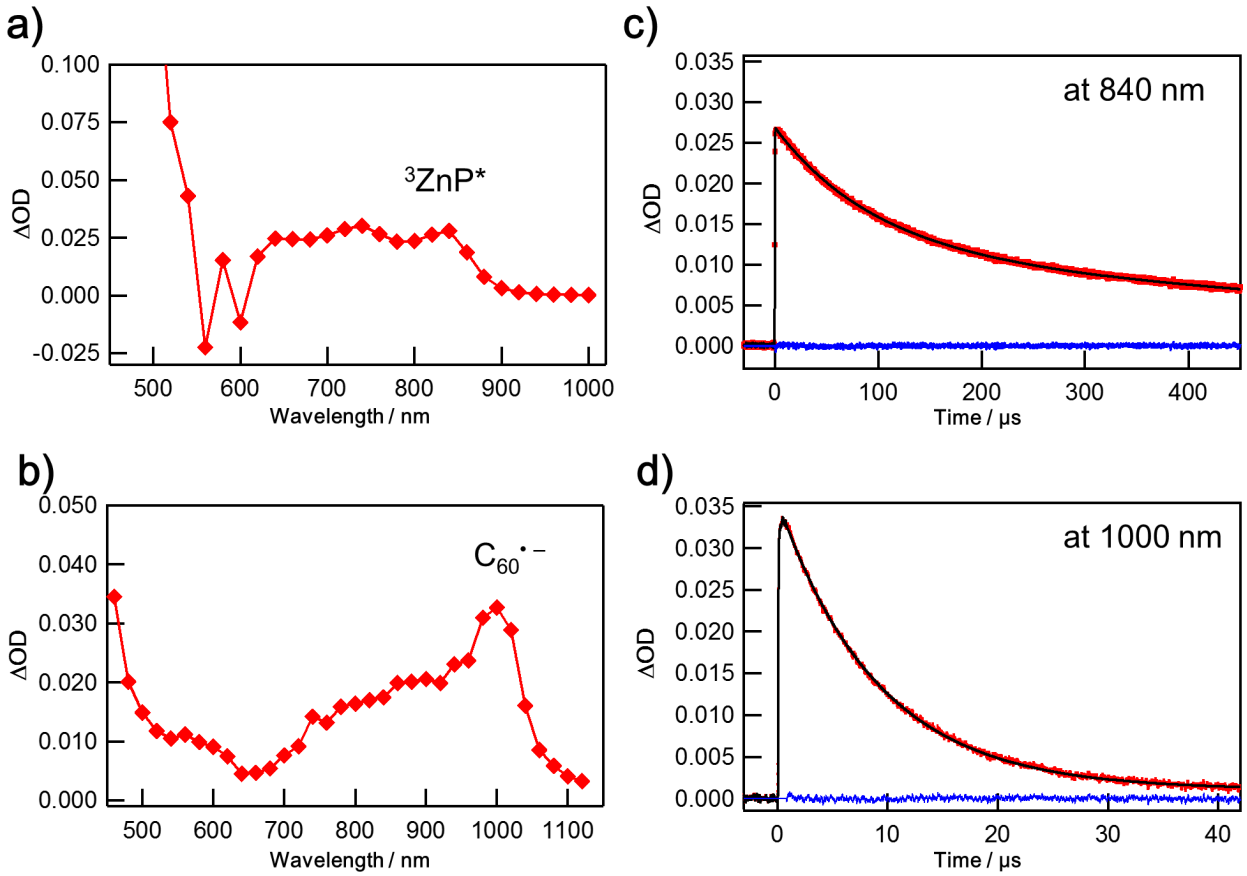

Fig. S11 Nanosecond time-resolved TA spectra of (a) **4** and (b) **5** in deaerated DMSO taken at 1.0 μs after laser excitation at 410 nm. Decay time profiles of (c) **4** at 840 nm arising from ^{3}ZnP* and (d) **5** at 1000 nm arising from $C_{60}^{\bullet -}$. Red plots are the observed signals, black line is drawn by the single-exponential or bi-exponential fitting, and blue line is the residual after the fitting. The lifetimes of ^{3}ZnP* are 92.8 μs (55%) and 622 μs (45%), where the values in parenthesis denote the ratio of the amplitudes. The lifetime of $C_{60}^{\bullet -}$ is 9.1 μs.

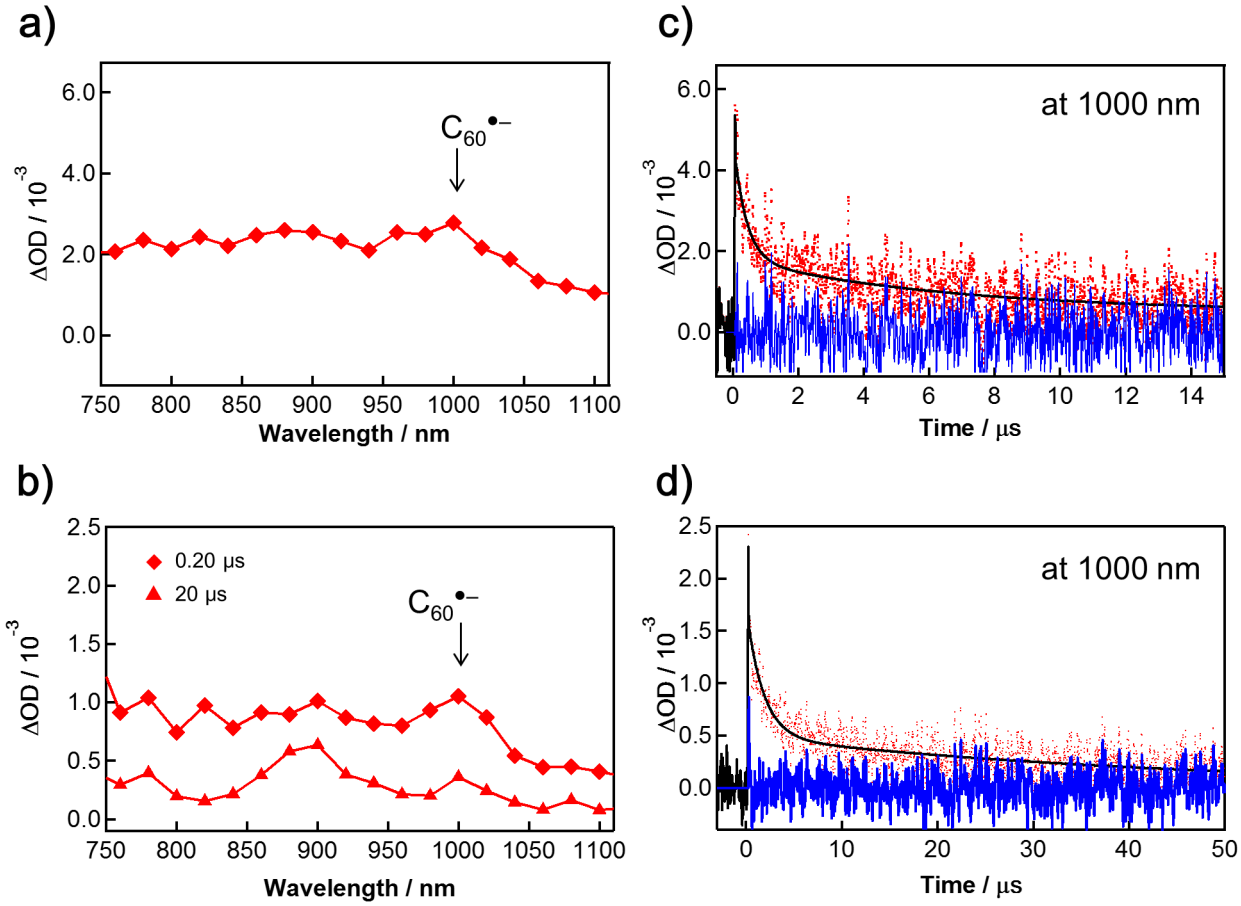

Fig. S12 (a) Nanosecond time-resolved TA spectra of **3** in deaerated DMSO/H_2O (1:99, v/v) and (b) in the lipid bilayer system using the liposome in H_2O taken at 0.30, 0.20 and 20 μs, after nanosecond laser excitation. The spectra were obtained by the excitation at 410 nm where the absorbances were adjusted to be identical (0.50). The decay time profiles at 1000 nm arising from $C_{60}^{\bullet-}$ of **3** (c) in deaerated DMSO/H_2O (1:99, v/v) and (d) in the lipid bilayer system in H_2O. Red plots are the observed signals, black line is drawn by the bi-exponential fitting, and blue line is the residual after the fitting.

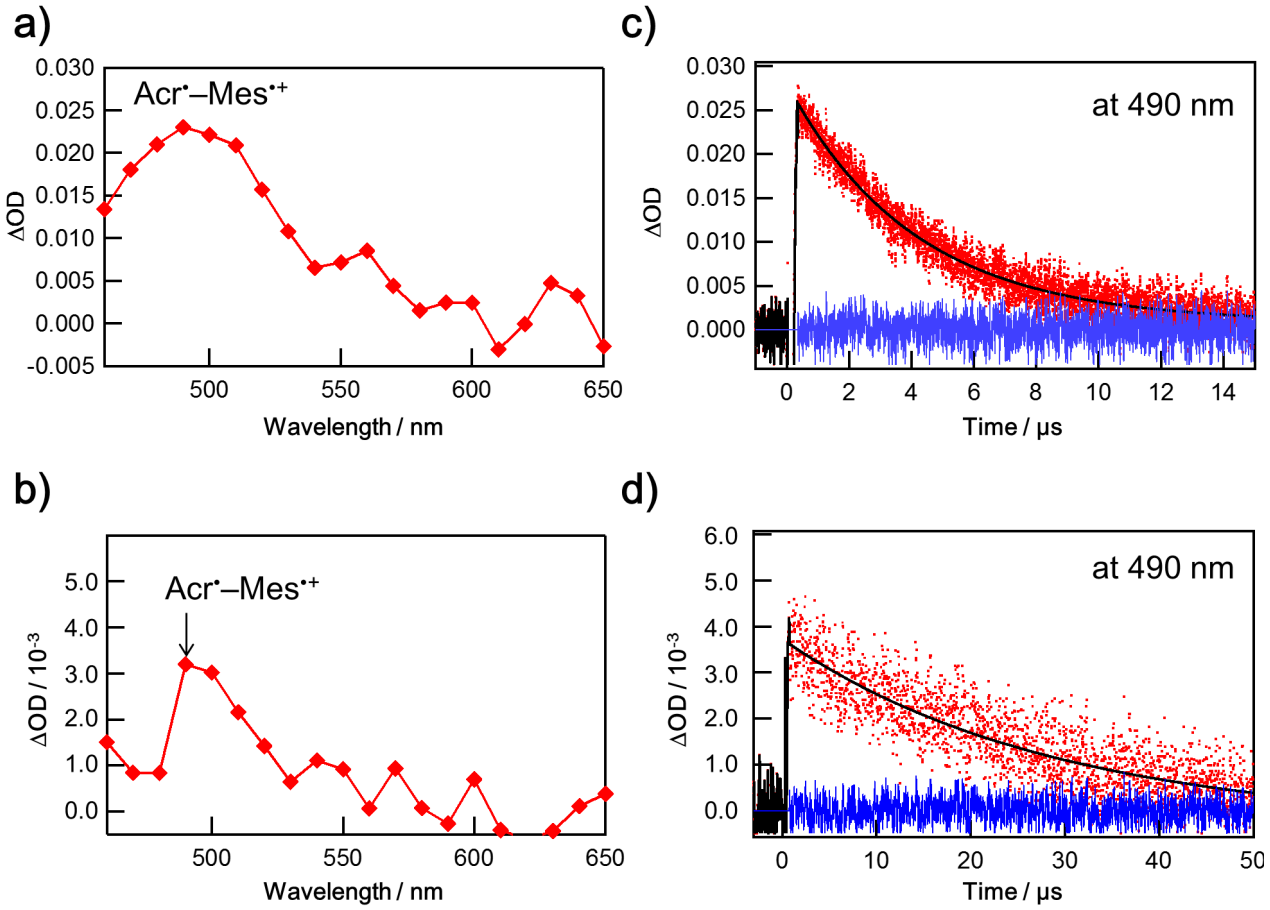

Fig. S13 (a) Nanosecond time-resolved TA spectrum of **7** in deaerated DMSO taken at 0.60 μs after laser excitation at 420 nm and (b) its decay time profile at 490 nm arising from acridinium radical ($Acr^{\bullet}$) and mesityl radical cation ($Mes^{\bullet+}$). (c) Nanosecond time-resolved TA spectrum of **7** in deaerated DMSO/H_2O (1:99, v/v) taken at 0.60 μs after laser excitation at 420 nm and (d) its decay time profile at 490 nm arising from $Acr^{\bullet}$-$Mes^{\bullet+}$. Red plots are the observed signals, black line is drawn by the single exponential fitting, and blue line is the residual after the fitting.

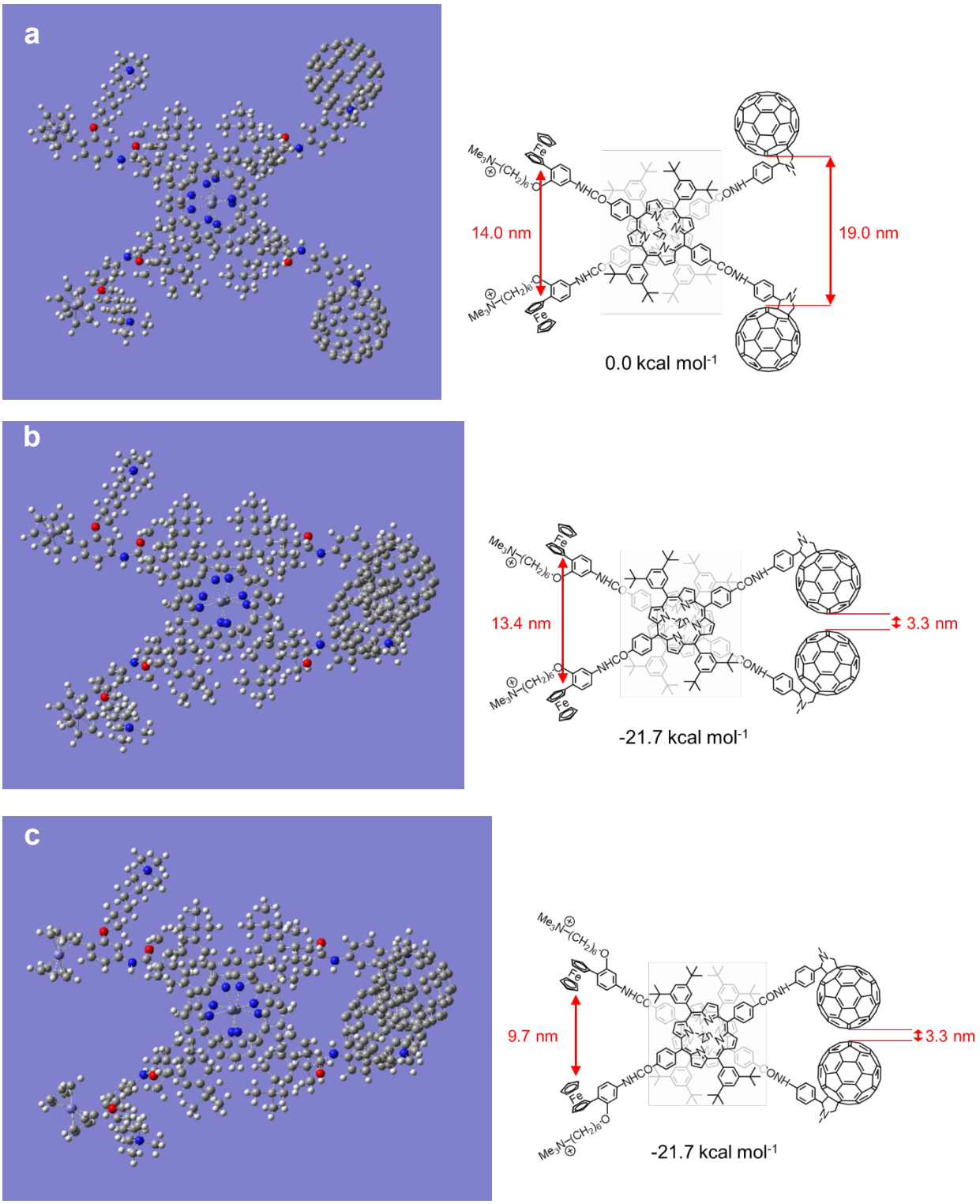

Fig. S14 DFT optimized plausible dimer structures of **1** calculated at the B3LYP-D3/6-31G(d) [C, H, N, O], LANL2DZ [Fe, Zn] level of theory (left) and their schematic drawings embedded with the relative energy of formation (right). (a) The two ferrocene moieties and the two fullerene moieties situated in the opposite side, (b) the two ferrocene moieties situated in the opposite side and the two fullerene moieties situated in the same side, and (c) the two ferrocene moieties and the two fullerene moieties situated in the same side. Embedded red allows and values in nm unit denote the separation distances between the two ferrocene moieties or the two fullerene moieties.

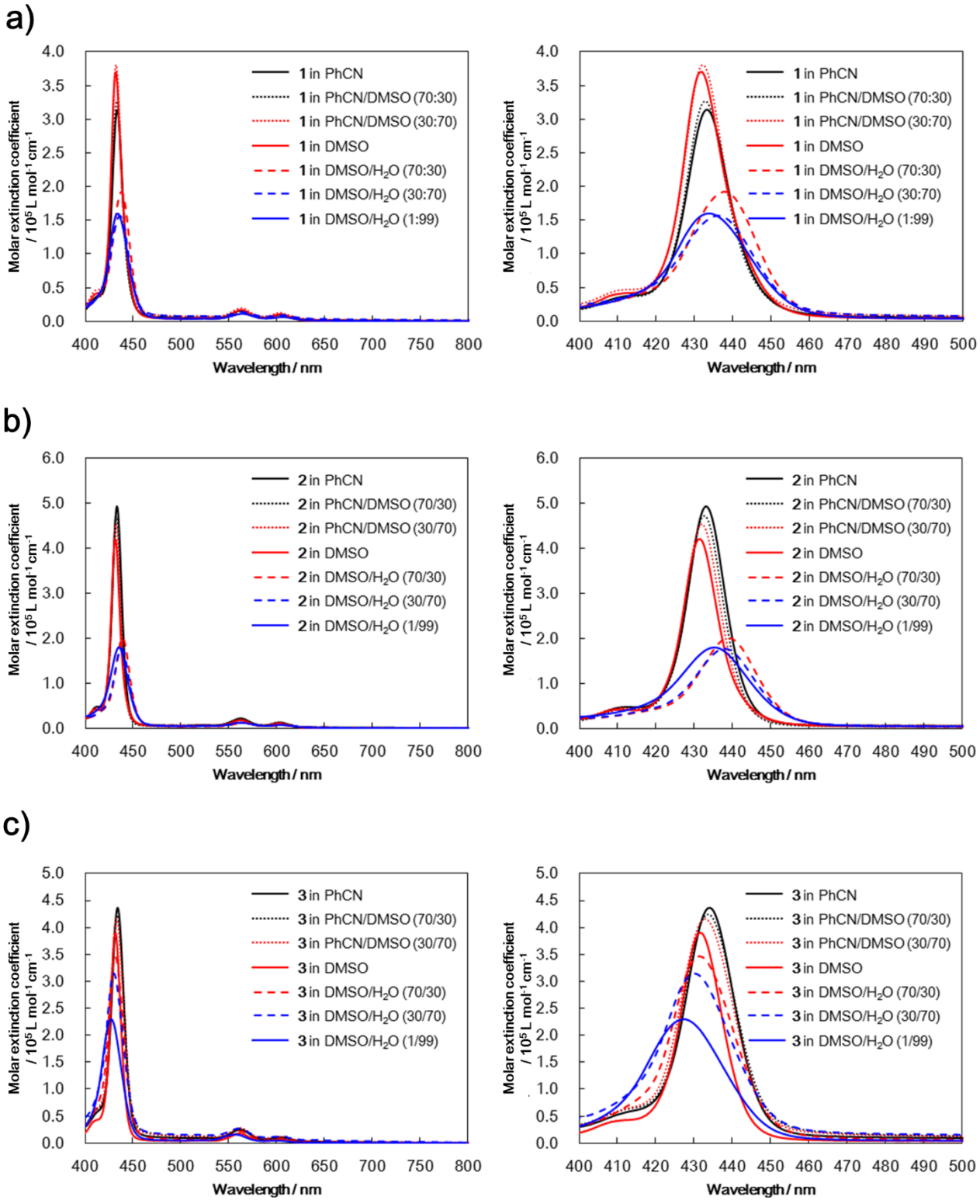

Fig. S15 UV-visible absorption spectra of (a) **1**, (b) **2** and (c) **3** in various solvents. Right figures show the expanded spectra.

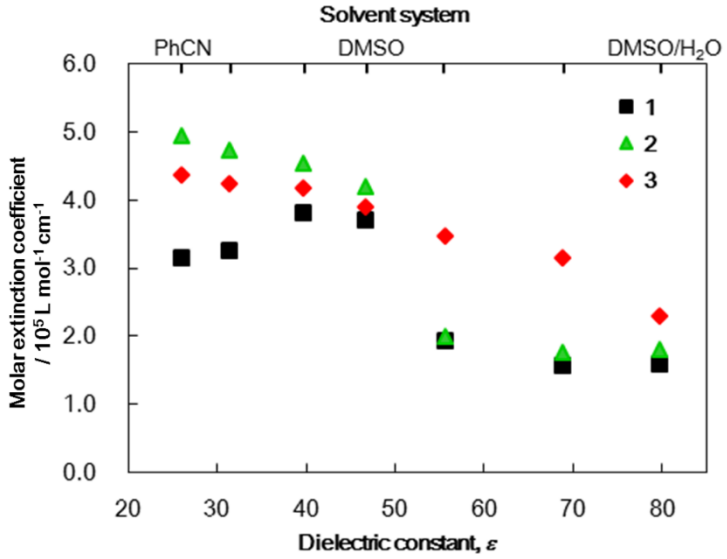

Fig. S16 Relation between the molar extinction coefficients at the Soret bands of **1**-**3** and dielectric constants of the various solvents, i.e., PhCN, PhCN/DMSO (70:30, v/v), PhCN/DMSO (30:70, v/v), DMSO, DMSO/H_2O (70:30, v/v), DMSO/H_2O (30:70, v/v) and DMSO/H_2O (1:99, v/v).

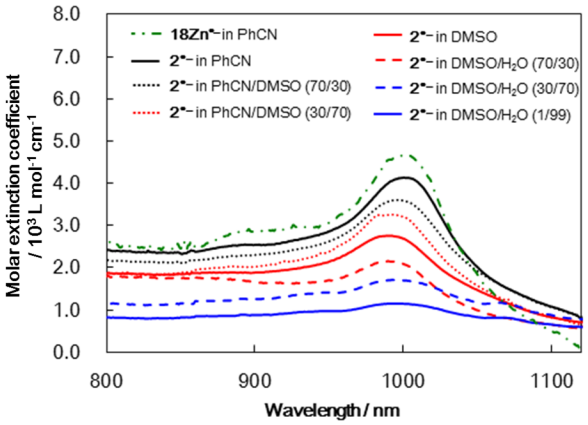

Fig. S17 Absorption spectra of $\mathbf{2}^{\bullet-}$ and the reference compound $\mathbf{18Zn}^{\bullet-}$ where one-electron reduced state of the C_{60} moiety is generated chemically by $(Me_2N)_4C_2$ in the various solvents.

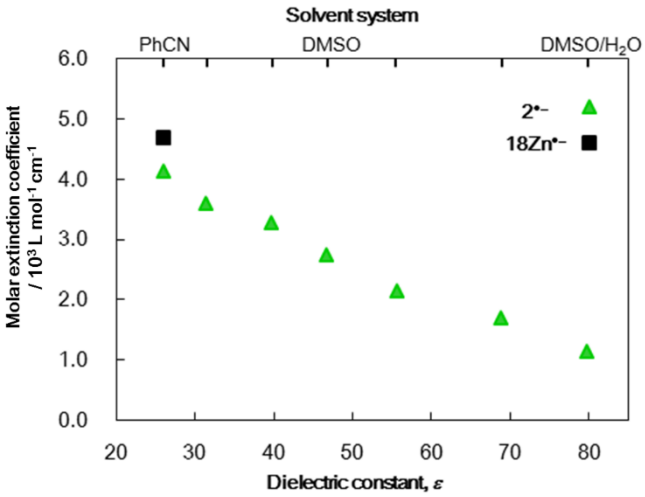

Fig. S18 Correlation between the molar extinction coefficients of $\mathbf{2}^{\bullet-}$ at 1000 nm and dielectric constants of the various solvents, i.e. PhCN, PhCN/DMSO (70:30, v/v), PhCN/DMSO (30:70, v/v), DMSO, DMSO/H_2O (70:30, v/v), DMSO/H_2O (30:70, v/v) and DMSO/H_2O (1:99, v/v).

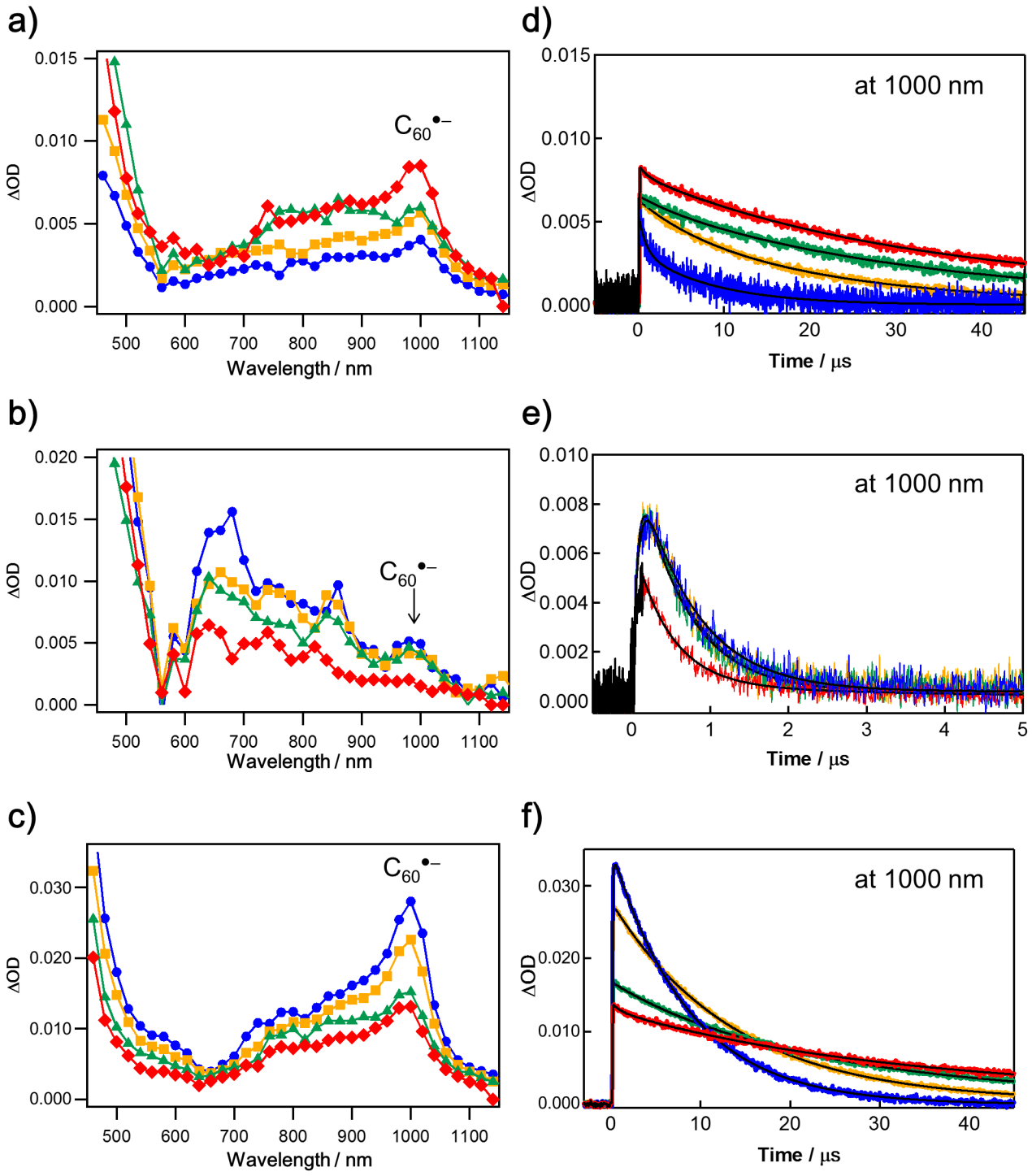

Fig. S19 Nanosecond time-resolved TA spectra of (a) **1**, (b) **2** and (c) **3** in deaerated (blue, ●) PhCN, (orange, ■) PhCN/DMSO (70:30, v/v), (green, ▲) PhCN/DMSO (30:70, v/v) and (red, ♦) DMSO taken at 1.0 μs, 0.30 μs and 1.5 μs, respectively, after nanosecond laser excitation. The spectra were obtained by the excitation at 410 nm where the absorbances were adjusted to be identical (0.50). Decay time profiles of (d) **1**, (e) **2** and (f) **3** at 1000 nm arising from $C_{60}^{\bullet-}$. Colored plots are the observed signals, while black line is drawn by the single-exponential or bi-exponential fitting.

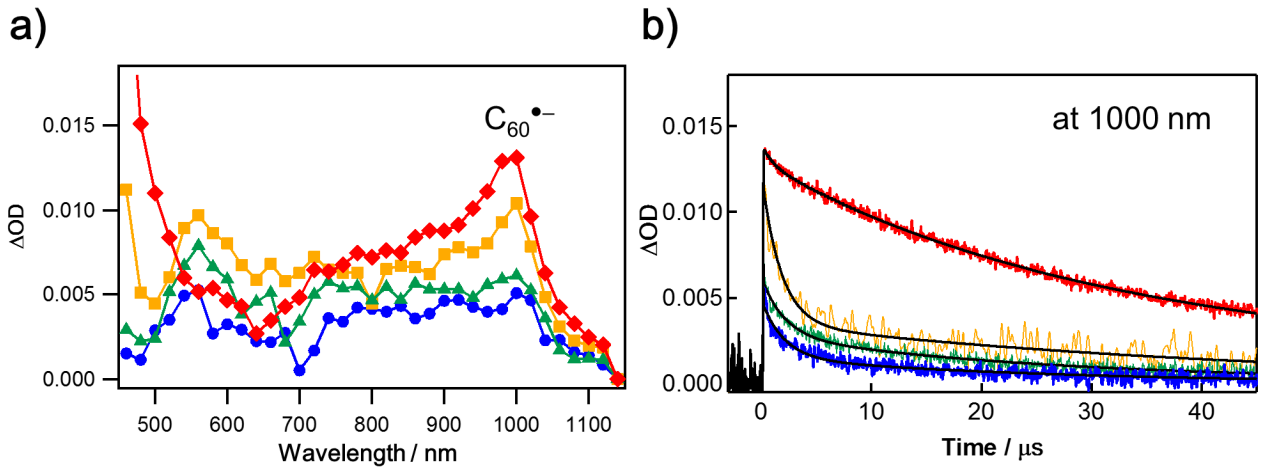

Fig. S20 (a) Nanosecond time-resolved TA spectra of **1** in deaerated (red, ♦) DMSO, (orange, ■) DMSO/H_2O (70:30, v/v), (green, ▲) DMSO/H_2O (30:70, v/v) and (blue, ●) DMSO/H_2O (1:99, v/v), taken at 1.5 μs, after nanosecond laser excitation. The spectra were obtained by the excitation at 410 nm where the absorbances were adjusted to be identical (0.50). (b) Decay time profiles at 1000 nm arising from $C_{60}^{\bullet-}$. Colored plots are the observed signals, while black line is drawn by the bi-exponential fitting.

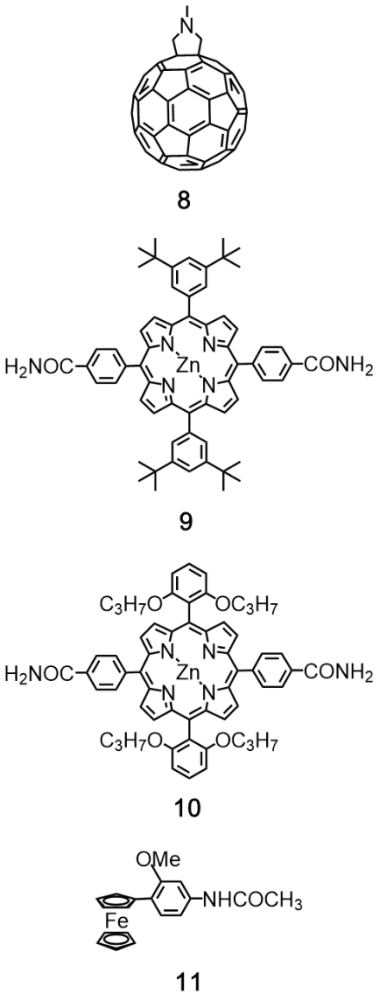

Fig. S21 Model molecular structures that were used for the theoretical calculations on the complexes.

a)

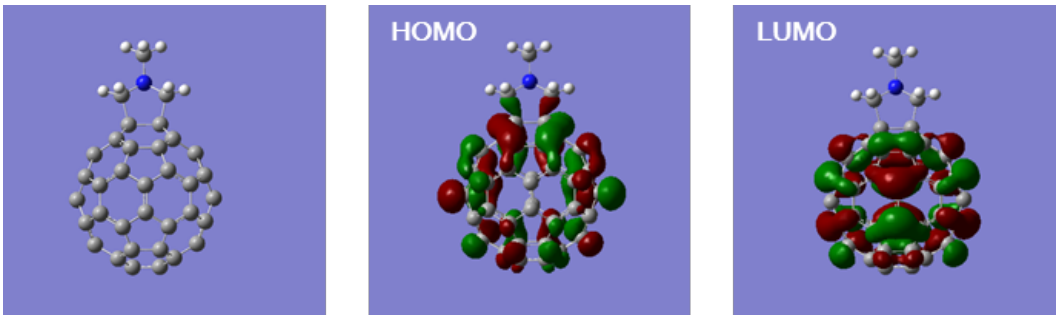

b)

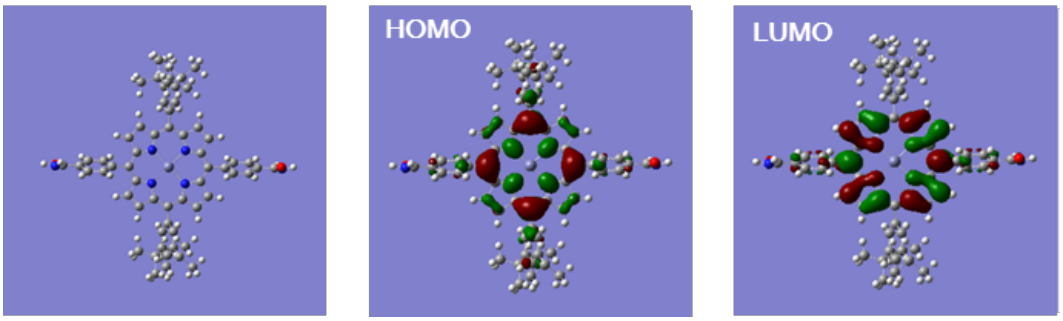

c)

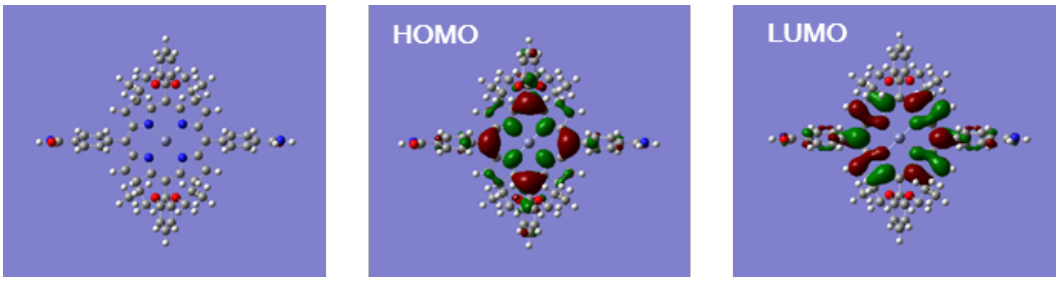

d)

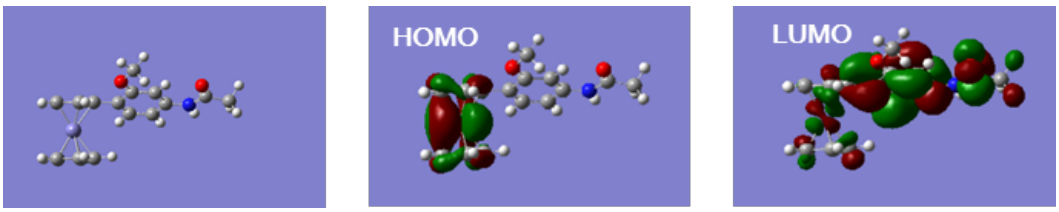

Fig. S22 DFT optimized structures (left), HOMO (center) and LUMO (right) of (a) **8**, (b) **9**, (c) **10** and (d) **11** calculated at the UB3LYP-D3/6-31G(d) [C, H, N, O], LANL2DZ [Fe, Zn] level of theory.

a)

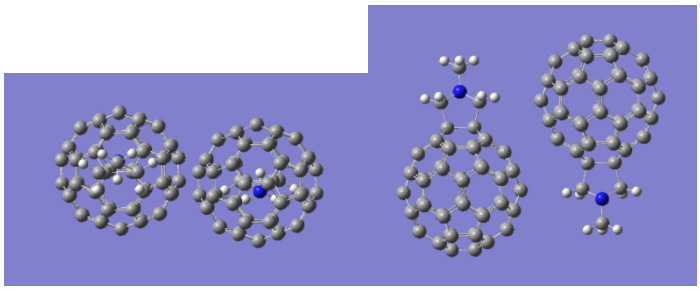

b)

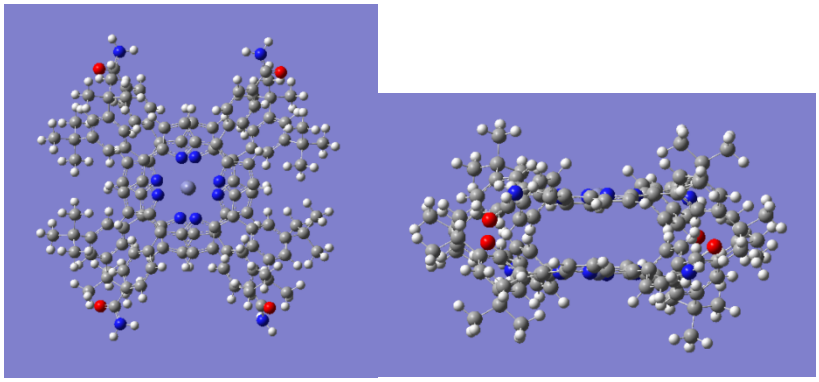

c)

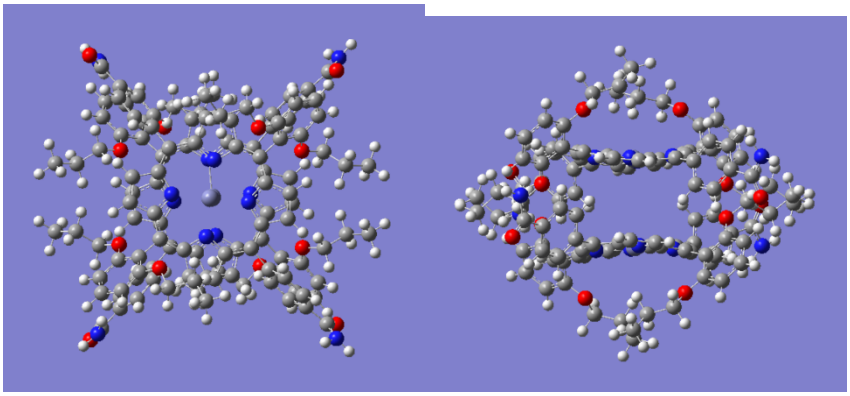

d)

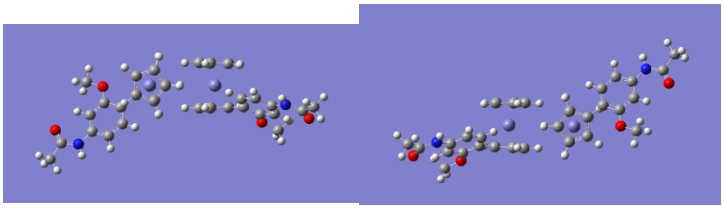

Fig. S23 Top view (left) and front view (right) of the DFT optimized structures of (a) **8**/**8**, (b) **9**/**9**, (c) **10**/**10** and (d) **11**/**11** calculated at the UB3LYP-D3/6-31G(d) [C, H, N, O], LANL2DZ [Fe, Zn] level of theory.

a)

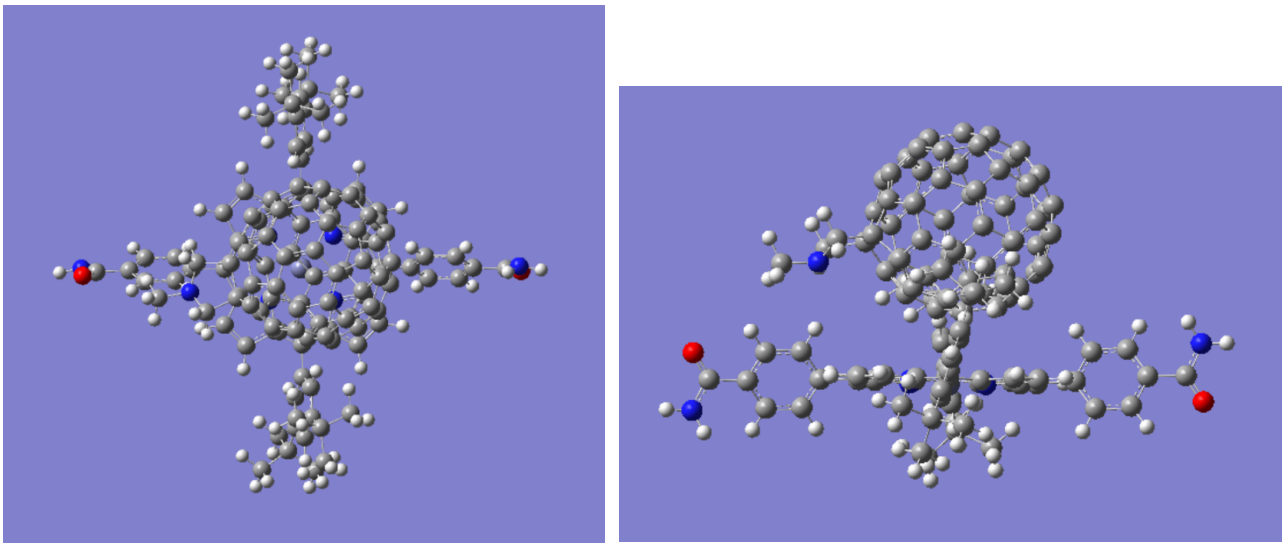

b)

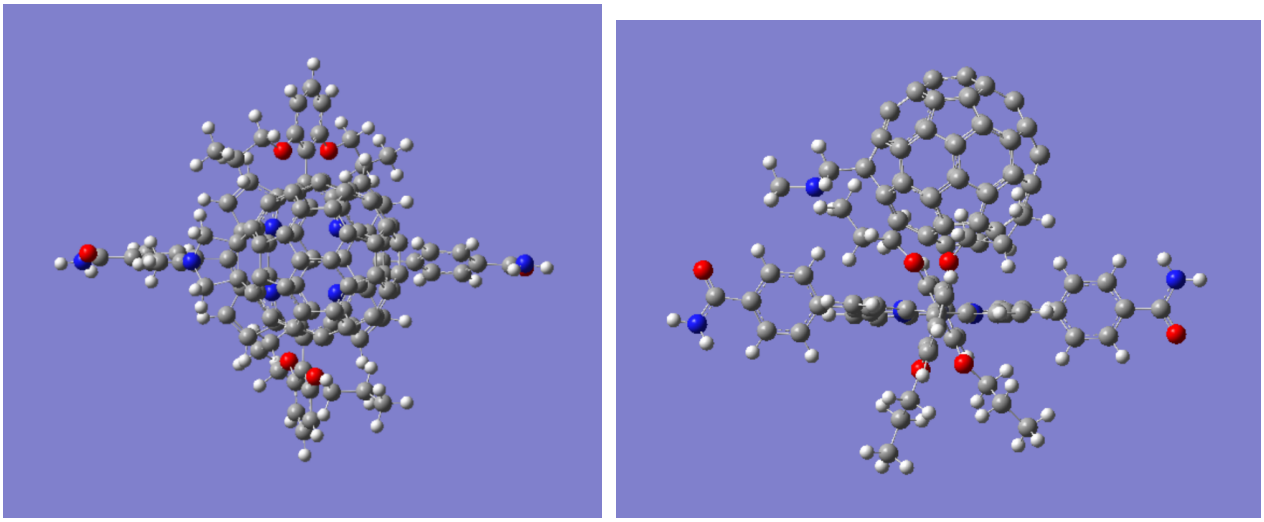

c)

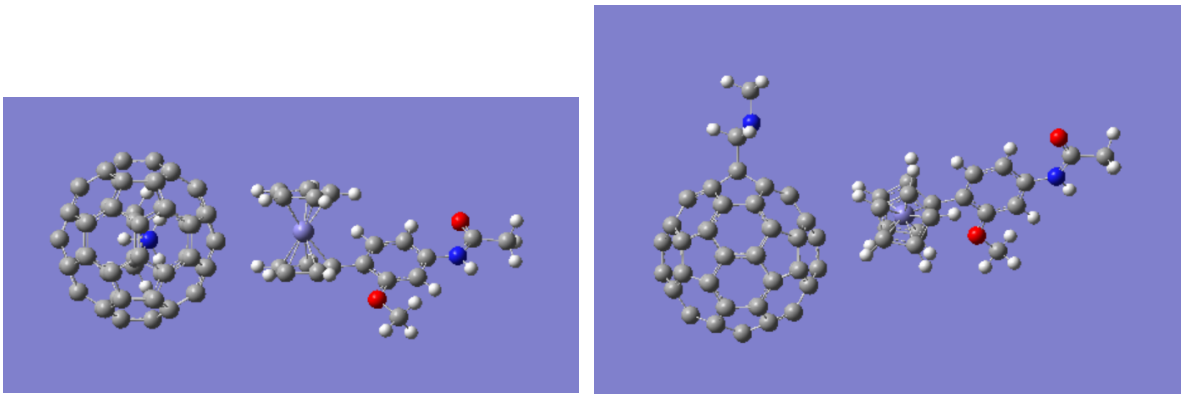

Fig. S24 Top view (left) and side view (right) of the DFT optimized structures of (a) **8**/**9**, (b) **8**/**10** and (c) **8**/**11** calculated at the UB3LYP-D3/6-31G(d) [C, H, N, O], LANL2DZ [Fe, Zn] level of theory.

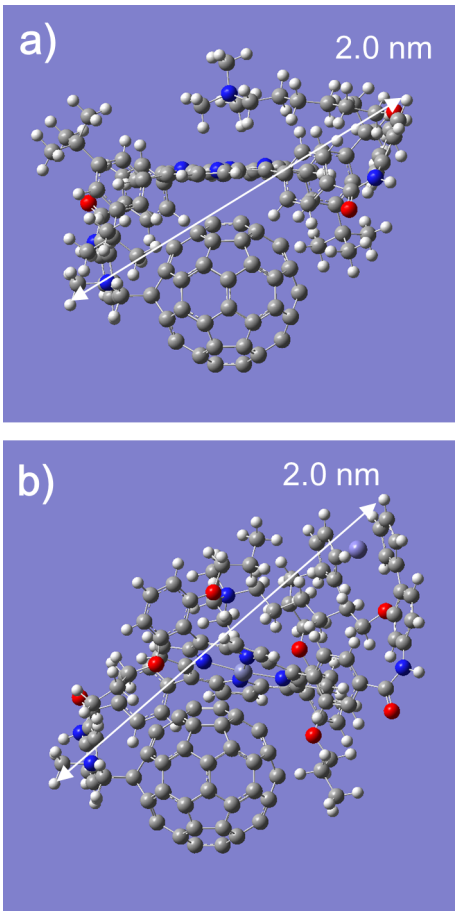

Fig. S25 DFT optimized structures of (a) **2** and (c) **3** in their packed structures where Br anion has been removed to simplify the calculation at the UB3LYP-D3/6-31G(d) [C, H, N, O], LANL2DZ [Fe, Zn] level of theory. Embedded white allows and values in nm unit denote the separation distances between the most distant pair of atoms.

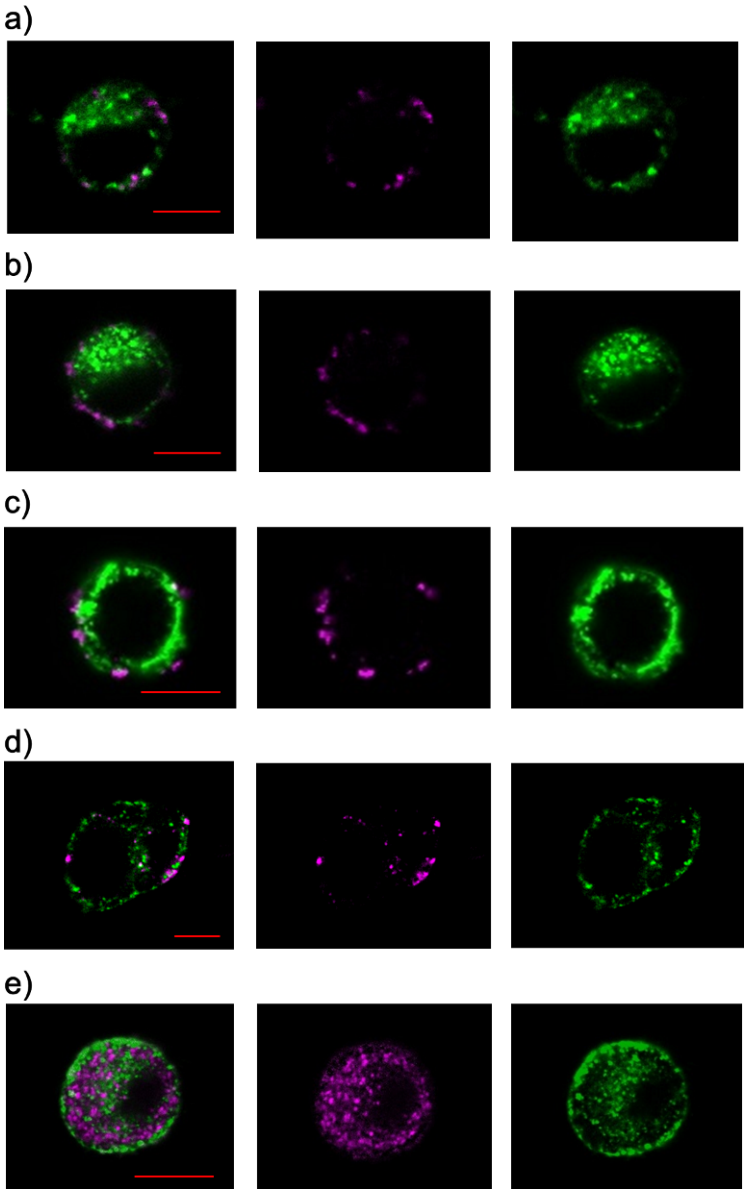

Fig. S26 Confocal microscopy images of PC12 cells that were stained by wheat germ agglutinin (WGA)-Alexa Fluor®488 conjugate and treated with (a) **1**, (b) **2**, (c) **3**, (d) **4** and (e) **7**. Merged image (left), where red bar indicates 5 μm, the compounds (magenta, center), and the Alexa Fluor488 conjugate (green, right). **1**, **2**, **3**, and **4** demonstrate dominant localization in/on the surface membrane, whereas **7** shows dominant localization in the endomembrane.

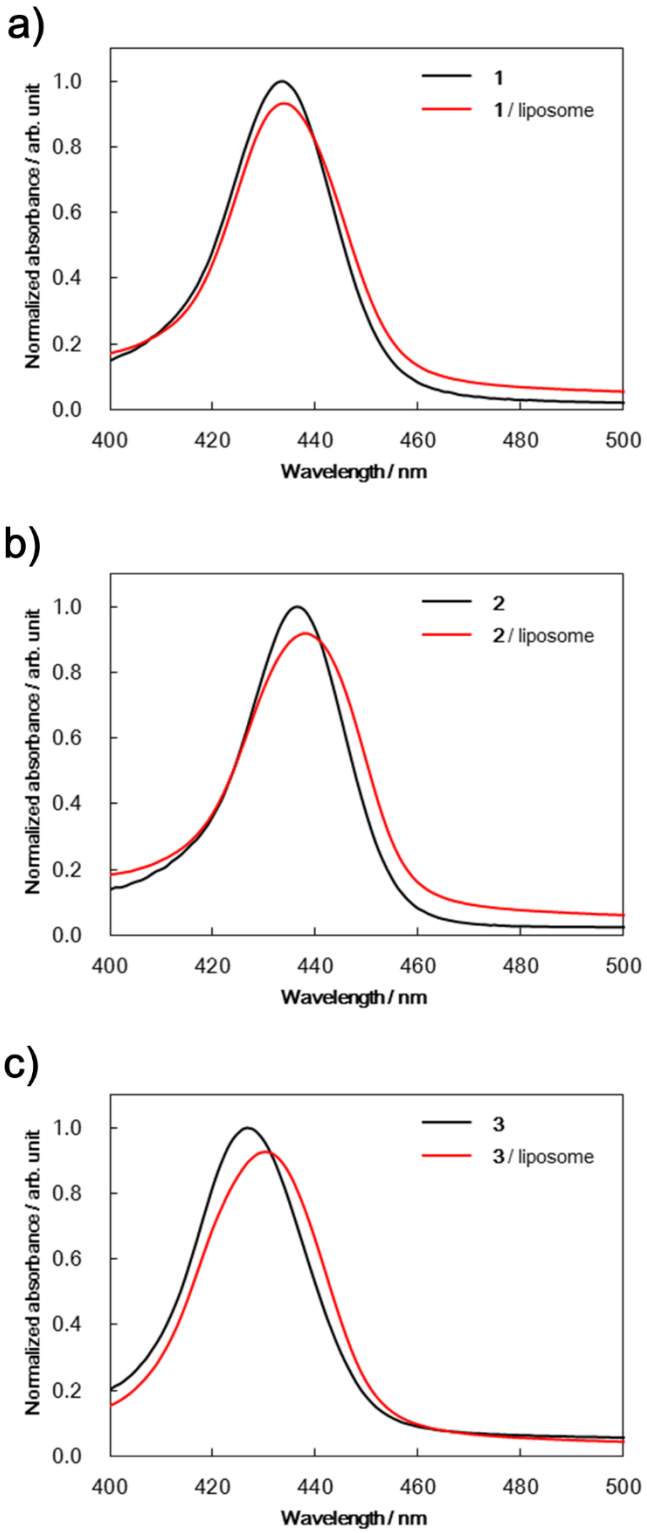

Fig. S27 UV-visible absorption spectra of (a) **1,** (b) **2** and (c) **3** in DMSO/H_2O (1:99, v/v) (black line) before and (red line) after the incorporation into the liposome.

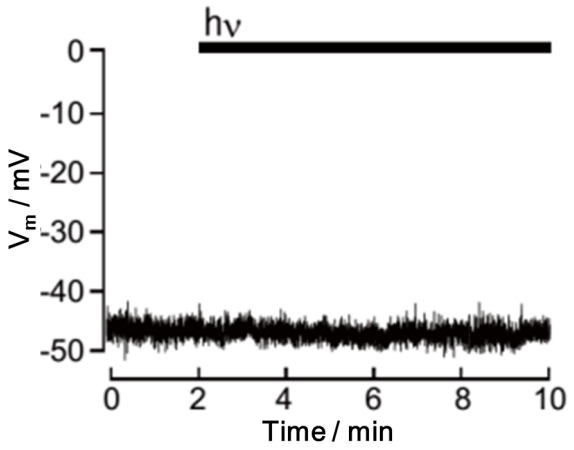

Fig. S28 Representative trace in the negative control condition (i.e. without any compounds) for the photoinduced depolarization in a PC12 cell by illumination (400−450 nm, 2.0 mW cm^{-2}).

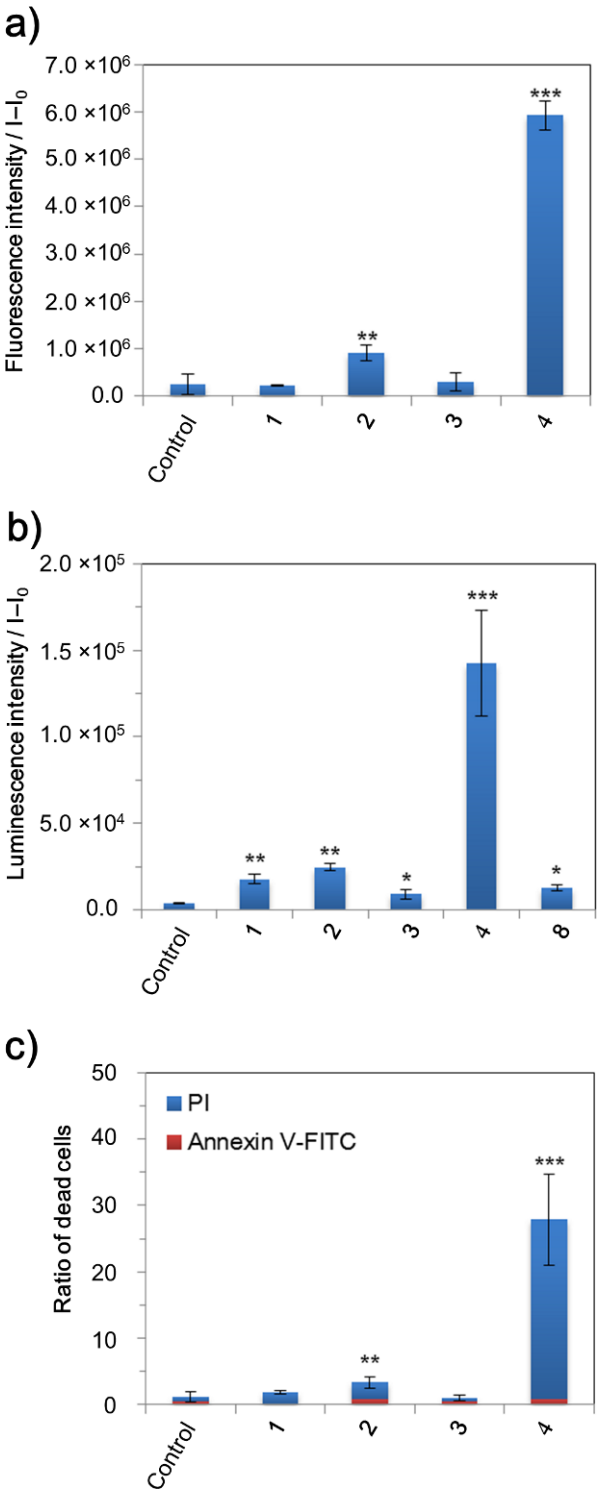

Fig. S29. ROS production and cell damage induction by illumination (400−450 nm, 2.0 mW cm^{-2}, 120 sec). (a) Detection of singlet oxygen by SOSG in DMSO/H_2O (1/99, v/v) and (b) detection of superoxide by MPEC in DMSO/H_2O. (c) Apoptosis/necrosis assay by using Annexine V-FITC/PI dyes. Blue bar and red bar in each column indicate the cells that were stained by PI (necrosis or late apoptosis) and by Annexine V-FITC (early apoptosis), respectively. Error bars denote S.D. (*n* = 3−4). Statistically significant differences between the negative control and each compound are indicated with asterisks (***P < 0.001, **P < 0.01, *P < 0.05).

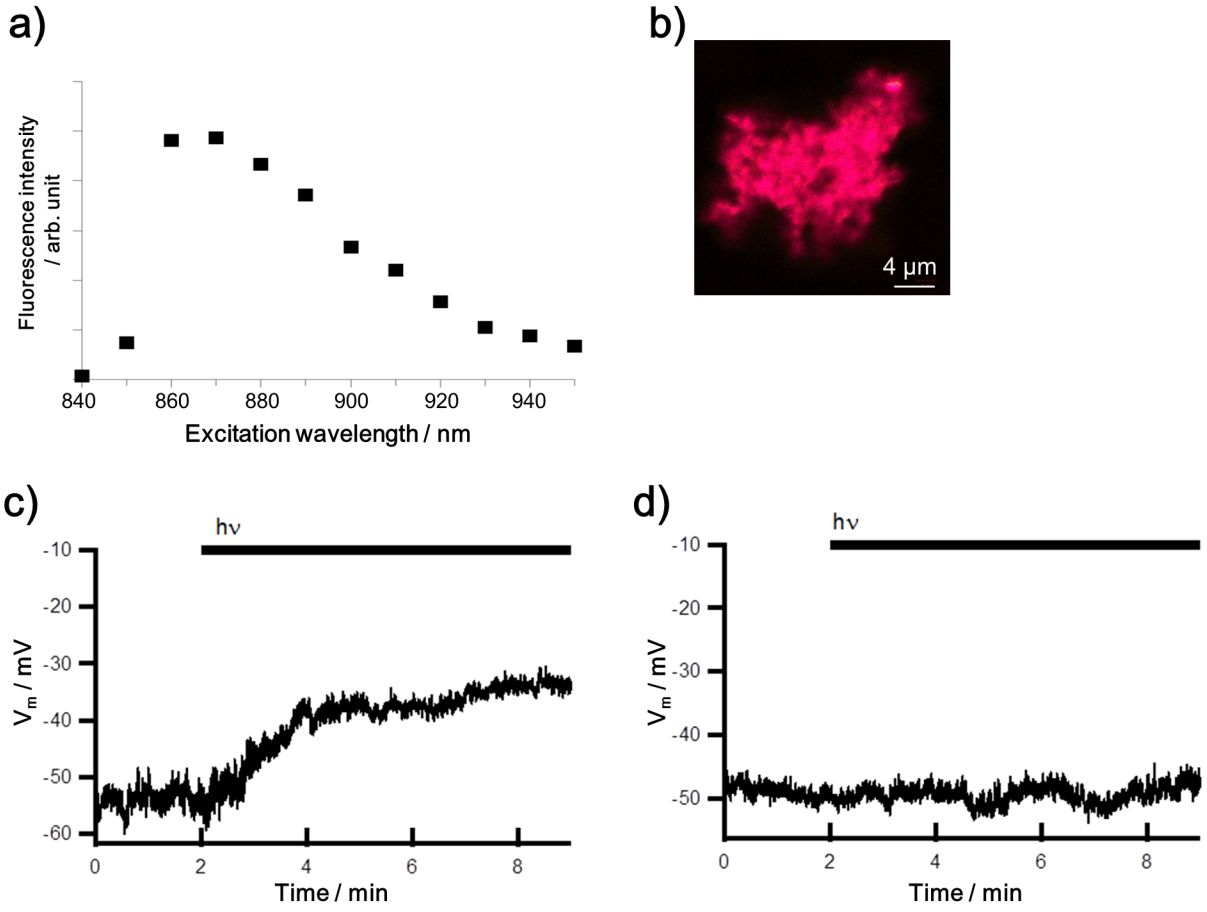

Fig. S30 (a) Excitation spectrum of fluorescence by the two-photon excitation on the aggregates of **3** recorded by the confocal laser microscopy with monitoring the range between 550-700 nm, and (b) a confocal fluorescence image of a large aggregate of **3**. Photoinduced depolarization in a PC12 cell membrane incorporated (c) with **3** and (d) without **3** by the two-photon excitation by pumped-pulse laser (*fs*-pulse, 860 nm, 250 mW cm^{-2} that is 6 μW on a cell).

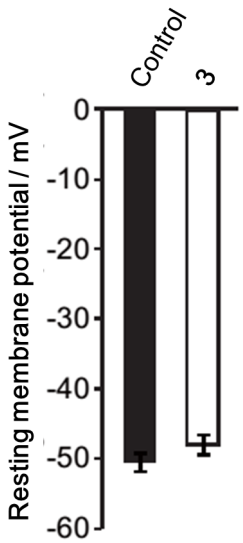

Fig. S31 Resting membrane potentials in rat hippocampal neurons obtained by the patch clamp measurements.

Table S1 Fluorescence lifetimes (τ).[a]

Compound	Medium	τ_1 (ps)	Relative amplitude (%)	τ_2 (ps)	Relative amplitude (%)
1[b]	DMSO	67	72	730	28
2[b]	DMSO	77	77	520	23
3[b]	DMSO	54	75	1100	25
4[c]	DMSO	1840	100		
5[d]	PhCN	95	100		
6[d]	PhCN	100	100		

(a) S.E. of the data shown here is less than 5%. (b) Data were obtained by up-conversion measurements. The excitation and monitoring wavelengths were 420 nm and 610 nm, respectively. (c) Data were obtained by single photon counting measurements. The excitation and monitoring wavelengths were 420 nm and 610 nm, respectively. (d) Data from ref 17.

Table S2. Complete data of the maximal differential absorbances (ΔOD_{max}), charge recombination kinetic constants (k_{CR}) and relative amplitudes in photoinduced charge-separated states in various solvent systems. [a]

Compd	Medium	ε_r [b]	ΔOD_{max} at 1000 nm	k_{CR1} (s^{-1})	Amplitude (%)	k_{CR2} (s^{-1})	Amplitude (%)	Φ_{CS}
1	PhCN	25.9	6.3×10^{-3}	1.2×10^{6}	40	1.2×10^{5}	60	0.15[d]
	PhCN/DMSO (70:30)	31.4[c]	5.8×10^{-3}	1.5×10^{5}	21	5.0×10^{4}	79	0.21[d]
	PhCN/DMSO (30:70)	39.7[c]	5.1×10^{-3}	2.4×10^{5}	7	3.1×10^{4}	93	0.24[d]
	DMSO	46.7	8.3×10^{-3}	1.4×10^{5}	15	2.2×10^{4}	85	0.38[d]
	DMSO/H_2O (70:30)	55.6[c]	n.d.[e]					
	DMSO/H_2O (30:70)	68.8[c]	n.d.[e]					
	DMSO/H_2O (1:99)	79.7[c]	n.d.[e]					
	Liposome in H_2O		n.d.[e]					
2	PhCN	25.9	7.6×10^{-3}	1.4×10^{6}	100			0.23[d]
	PhCN/DMSO (70:30)	31.4[c]	7.4×10^{-3}	1.6×10^{6}	100			0.25[d]
	PhCN/DMSO (30:70)	39.7[c]	7.5×10^{-3}	1.6×10^{6}	100			0.29[d]
	DMSO	46.7	2.8×10^{-3}	1.5×10^{6}	43	2.9×10^{5}	57	0.12[d]
	DMSO/H_2O (70:30)	55.6[c]	n.d.[e]					
	DMSO/H_2O (30:70)	68.8[c]	n.d.[e]					
	DMSO/H_2O (1:99)	79.7[c]	n.d.[e]					
	Liposome in H_2O		n.d.[e]					
3	PhCN	25.9	3.3×10^{-2}	1.2×10^{5}	100			0.99[d,f]
	PhCN/DMSO (70:30)	31.4[c]	2.8×10^{-2}	7.7×10^{4}	100			0.95[d]
	PhCN/DMSO (30:70)	39.7[c]	1.7×10^{-2}	2.2×10^{5}	4	4.2×10^{4}	96	0.63[d]
	DMSO	46.7	1.4×10^{-2}	7.7×10^{4}	17	2.5×10^{4}	83	0.62[d]
	DMSO/H_2O (70:30)	55.6[c]	1.1×10^{-2}	5.0×10^{5}	49	3.0×10^{4}	51	0.63[d]

	DMSO/H_2O (30:70)	68.8[c]	6.9×10^{-3}	1.5×10^{6}	52	7.7×10^{4}	48	0.58[d]
	DMSO/H_2O (1:99)	79.7[c]	5.5×10^{-3}	2.6×10^{6}	66	1.6×10^{5}	34	0.57[d]
	Liposome in H_2O		2.3×10^{-3}	5.9×10^{5}	68	2.2×10^{4}	32	0.27[d]
5	PhCN	25.9	3.3×10^{-2}	1.1×10^{5}	100			0.99[g]
7[h]	MeCN	37.5	2.8×10^{-2}	2.4×10^{5}	100			0.98[i]
	DMSO/H_2O (1:99)	79.7	4.2×10^{-3}	3.5×10^{4}	100			0.37[j]

(a) S.E. of the data shown here is less than 5%. (b) Data from ref 21. (c) Value determined by using the Bruggeman equation as described in ref 22. (d) Value obtained by comparison of the maximum intensity at 1000 nm taking into account of the different molar extinction coefficients caused by the solvent systems (Table S4). (e) Not determined because of the low s/n ratio. (f) The extinction coefficient of $18Zn^{\bullet-}$ was used considering the existence of **3** as a non-aggregated form in PhCN. (g) Data from ref 17. (h) Value obtained by the maximum intensity at 490 nm, arising from the corresponding radical ion pair. (i) Data from ref 23. (j) Value obtained by the maximum intensity at 490 nm with that of **7** taking into account of the different extinction coefficients caused by the solvent systems.

Table S3. Solvent dependence of peak wavelengths (λ) and molar extinction coefficients (*ε*) of the Soret band and mean particle size in the solutions. Mean particle size below 5 nm may result from the small aggregates or monomeric-like molecules based on the DFT optimized structures (Figs. S6 and S25).

Compound	Medium[a]	ε_r[b]	λ_{Soret} (nm)	ε_{Soret} (10^5 L mol^{-1} cm^{-1})	Mean particle size[c]
1	PhCN	25.9	433	3.1	8 ± 1
	PhCN/DMSO (70:30)	31.4[d]	433	3.3	8 ± 1
	PhCN/DMSO (30:70)	39.7[d]	432	3.8	5 ± 1
	DMSO	46.7	431	3.7	7 ± 2
	DMSO/H_2O (70:30)	55.6[d]	438	1.9	9 ± 2
	DMSO/H_2O (30:70)	68.8[d]	436	1.6	19 ± 2
	DMSO/H_2O (1:99)	79.7[d]	434	1.6	60 ± 49
	Liposome in H_2O		434	1.5	
2	PhCN	25.9	433	4.9	4 ± 1
	PhCN/DMSO (70:30)	31.4[d]	433	4.7	4 ± 1
	PhCN/DMSO (30:70)	39.7[d]	432	4.5	4 ± 1
	DMSO	46.7	431	4.2	5 ± 2
	DMSO/H_2O (70:30)	55.6[d]	439	2.0	8 ± 1
	DMSO/H_2O (30:70)	68.8[d]	438	1.8	21 ± 8
	DMSO/H_2O (1:99)	79.7[d]	435	1.8	46 ± 41
	Liposome in H_2O		438	1.7	
3	PhCN	25.9	434	4.4	4 ± 1
	PhCN/DMSO (70:30)	31.4[d]	434	4.2	4 ± 1
	PhCN/DMSO (30:70)	39.7[d]	433	4.1	4 ± 1
	DMSO	46.7	432	3.9	11 ± 2
	DMSO/H_2O (70:30)	55.6[d]	432	3.5	20 ± 4
	DMSO/H_2O (30:70)	68.8[d]	430	3.2	35 ± 14
	DMSO/H_2O (1:99)	79.7[d]	427	2.3	80 ± 21
	Liposome in H_2O		430	2.1	

(a) v/v. (b) Data from ref 21. (c) Data were obtained by DLS measurements based on the number distribution. (d) Value determined by using the Bruggeman equation as described in ref 22.

Table S4. Molar extinction coefficients of anion radicals in various solvents. Difference in the molar extinction coefficients of $\mathbf{2}^{\bullet-}$ and $\mathbf{18Zn}^{\bullet-}$ is attributed to the influence of the aggregation in $\mathbf{2}^{\bullet-}$, because the molar extinction coefficient of $\mathbf{18Zn}^{\bullet-}$ is comparable to that of mono-functionalized C_{60} derivatives in PhCN (ε = 4.7).[24]

Compound	Medium[a]	ε_r[b]	ε_{1000nm} (10^3 L mol^{-1} cm^{-1})
$\mathbf{2}^{\bullet-}$	PhCN	25.9	4.1
	PhCN/DMSO (70:30)	31.4[c]	3.6
	PhCN/DMSO (30:70)	39.7[c]	3.2
	DMSO	46.7	2.7
	DMSO/H_2O (70:30)	55.6[c]	2.0
	DMSO/H_2O (30:70)	68.8[c]	1.7
	DMSO/H_2O (1:99)	79.7[c]	1.2
	Liposome in H_2O		1.1[d]
$\mathbf{18Zn}^{\bullet-}$	PhCN	25.9	4.7

(a) v/v. (b) Data from ref 21. (c) Value determined by using the Bruggeman equation as described in ref 22. (d) Value estimated from the difference between the molar extinction coefficients of **1**-**3** in DMSO/H_2O (1:99, v/v) and that in the liposome.

Table S5. Binding energies of the complexes.[a] In the ground state, binding energies of the dimer of the porphyrins having *tert*-butyl groups (**9**/**9**) are found to be the most considerable. Therefore the strongest aggregations, which can accelerate deactivation of the excited-states, are expected for **1** and **2**. The binding energy is destabilized by 10 kcal mol^{-1} in the dimer of the porphyrins having decanoxy groups (**10**/**10**), which corresponds to the porphyrin part of **3**. This difference in energies was significantly large to rationalize the difference in the substituent effects that were observed and discussed in the present study. Although one can consider that the porphyrin/fullerene interaction (**8**/**9** and **8**/**10**) might be considerable, the calculations suggest that they are much smaller interaction than those of **9**/**9** or **10**/**10**, which is supported by the fact that no remarkable charge-transfer band was observed in the absorption spectra of **1**–**3**. It was also confirmed by the calculations with the PCM model that solvent effects do not have an influence on the order of the binding energies.

	ΔE (kcal mol^{-1})	BSSE ΔE (kcal mol^{-1})	Raw ΔE[b] (kcal mol^{-1})	PCM ΔE in DMSO[b] (kcal mol^{-1})	PCM ΔE in DMSO/H_2O[b] (kcal mol^{-1})
8/**8**	–9.7	2.1	–11.8	–11.0	–11.0
9/**9**	–44.5	13.9	–57.4	–52.9	–52.9
10/**10**	–34.5	12.6	–47.1	–40.4	–40.6
11/**11**	–7.7	2.0	–9.7	–9.0	–8.7
8/**9**	–26.8	7.1	–33.9	–28.8	–28.8
8/**10**	–24.1	7.7	–31.8	–25.8	–25.7
8/**11**	–4.3	1.5	–5.8	–6.5	–6.5

(a) Energies calculated at the UB3LYP-D3/6-311G(d) [6-311+G(d) for N atoms and LANL2DZ for Fe and Zn atoms] with BSSE correction by the counter poise method, using geometries optimized with UB3LYP-D3/6-31G(d) [LANL2DZ for Fe and Zn]. (b) Energies without BSSE correction.

Table S6. Spin densities, intermolecular distances, and binding energies[a] of complexes where either component is charged in the pair. In the all cases that either component is charged in the pair, the binding energies are decreased in comparison with the corresponding neutral state.

	Spin densities	Intermolecular distance (Å)[b]	ΔE (kcal mol^{-1})	BSSE ΔE (kcal mol^{-1})	ΔE *vs.* neutral complexes[c] (kcal mol^{-1})
[8/8]$^{\bullet-}$	0.500/0.500	3.2	–17.8	2.5	–9.0
8/9$^{\bullet+}$	0.036/0.964	3.2	–31.1	7.5	–6.1
8/11$^{\bullet+}$	0.001/0.999	4.0	–31.6	1.5	–26.8
8$^{\bullet-}$/9	0.982/0.018	3.3	–31.2	7.6	–5.9
8$^{\bullet-}$/10	0.984/0.016	3.3	–25.6	8.1	–3.3
8$^{\bullet-}$/11	0.998/0.002	4.1	–5.6	1.8	–1.2
[9/9]$^{\bullet+}$	0.500/0.500	4.1	–56.4	13.6	–10.5
11/11$^{\bullet+}$	0.000/1.000	4.8	–33.6	2.0	–10.2

(a) Energies calculated at the UB3LYP-D3/6-311G(d) [6-311+G(d) for N atoms and LANL2DZ for Fe and Zn atoms] with BSSE correction by the counter poise method, using geometries optimized with UB3LYP-D3/6-31G(d) [LANL2DZ for Fe and Zn]. (b) Distance between the nearest atoms that possess the SOMO and/or LUMO. (c) ΔE of the neutral complexes are shown on Table S5.

Table S7. Spin densities, intermolecular distances, and binding energies of complexes where charge-separated states are formed by both the components.[a] In the case that the charge-separated state is formed by the two molecules, the destabilization occurs between the same types of the molecules having the same charge (**8**$^{\bullet-}$/**8**$^{\bullet-}$, **9**$^{\bullet+}$/**9**$^{\bullet+}$ and **11**$^{\bullet+}$/**11**$^{\bullet+}$), whereas the stabilization does between the D-A types having the opposite charges (**8**$^{\bullet-}$/**9**$^{\bullet+}$ and **8**$^{\bullet-}$/**11**$^{\bullet+}$). Moreover, it is noteworthy that the stabilization energies of **8**$^{\bullet-}$/**9**$^{\bullet+}$ and **8**$^{\bullet-}$/**11**$^{\bullet+}$ are considerably higher than those of **8**/**9**$^{\bullet+}$, **8**$^{\bullet-}$/**9**, **8**/**11**$^{\bullet+}$ or **8**$^{\bullet-}$/**11** (Table S6). This result suggests that the intermolecular CR may occur in the aggregates by the reorientation of the charge-separated states in the aggregates when they are excited by the pulsed laser or continuous irradiation as used in the present study. Consequently, the CR is the most probable in the aggregates of **2** on the basis of the large binding energy and the short intermolecular distance of **8**$^{\bullet-}$/**9**$^{\bullet+}$. These results are in good agreement with the CS yield of the observed charge-separated states (Fig. 2 and Table 3).

	Spin densities	Intermolecular distance (Å)[b]	ΔE (kcal mol^{-1})	BSSE ΔE (kcal mol^{-1})
8$^{\bullet-}$/**8**$^{\bullet-}$	1.000/1.000	3.2	15.9	2.6
8$^{\bullet-}$/**9**$^{\bullet+}$	0.752/1.248	3.2	–81.8	8.7
8$^{\bullet-}$/**11**$^{\bullet+}$	0.521/1.479	3.9	–77.5	1.7
9$^{\bullet+}$/**9**$^{\bullet+}$	1.000/1.000	4.1	–21.5	13.0
11$^{\bullet+}$/**11**$^{\bullet+}$	1.000/1.000	6.9	19.6	0.9

(a) Data were calculated at the UB3LYP-D3/6-311G(d) [6-311+G(d) for N atoms and LANL2DZ for Fe and Zn atoms] with BSSE correction by the counter poise method, using geometries optimized with UB3LYP-D3/6-31G(d) [LANL2DZ for Fe and Zn]. (b) Distance between the nearest atoms that possess the SOMO and/or LUMO.

Table S8. Number of the incorporated molecules in a cell.

Compound	Number per a single cell (10^6 molecules)[a]
1	5.0 ± 0.1
2	5.4 ± 0.1
3	2.5 ± 0.3
4	23.6 ± 1.4

(a) Data are the mean values ± S.E. of three independent experiments.